

Article

Evolution of temperature preference in flies of the genus *Drosophila*

<https://doi.org/10.1038/s41586-025-08682-z>

Received: 8 December 2023

Accepted: 22 January 2025

Published online: 5 March 2025

 Check for updates

Matthew Capek¹, Oscar M. Arenas^{1,3}, Michael H. Alpert^{1,2}, Emanuela E. Zaharieva¹, Iván D. Méndez-González¹, José Miguel Simões^{1,4}, Hamin Gil¹, Aldair Acosta¹, Yuqing Su¹, Alessia Para^{1,5} & Marco Gallio^{1,2,6}

The preference for a particular thermal range is a key determinant of the distribution of animal species. However, we know little on how temperature preference behaviour evolves during the colonization of new environments. Here we show that at least two distinct neurobiological mechanisms drive the evolution of temperature preference in flies of the genus *Drosophila*. Fly species from mild climates (*D. melanogaster* and *D. persimilis*) avoid both innocuous and noxious heat, and we show that the thermal activation threshold of the molecular heat receptor Gr28b.d precisely matches species-specific thresholds of behavioural heat avoidance. We find that desert-dwelling *D. mojavensis* are instead actively attracted to innocuous heat. Notably, heat attraction is also mediated by Gr28b.d (and by the antennal neurons that express it) and matches its threshold of heat activation. Rather, the switch in valence from heat aversion to attraction correlates with specific changes in thermosensory input to the lateral horn, the main target of central thermosensory pathways and a region of the fly brain implicated in the processing of innate valence^{1–5}. Together, our results demonstrate that, in *Drosophila*, the adaptation to different thermal niches involves changes in thermal preference behaviour, and that this can be accomplished using distinct neurobiological solutions, ranging from shifts in the activation threshold of peripheral thermosensory receptor proteins to a substantial change in the way temperature valence is processed in the brain.

On the timescale of evolution, adaptation to new thermal environments is usually thought of as a set of coordinated changes in biochemistry and physiology that make it possible for a species to tolerate and eventually thrive in new thermal conditions. Likewise, resilience or vulnerability to rapid climate change is often portrayed as the ability (or lack of ability) to physiologically adapt to changes in climate. Yet, for animals that are able to move and migrate, behavioural responses to temperature (and temperature preference in particular) are at the forefront of their interactions with the environment. As a consequence, changing temperatures can alter the distribution and migratory routes of many species, even before directly threatening their survival (for example, refs. 6,7). We know little on how the species-specific preference for a particular thermal habitat is determined, or on how thermal preference changes as an animal adapts to a new environment. Here we study the evolution of temperature preference behaviour using *Drosophila* species representing adaptation to diverse thermal environments, ranging from cool high-altitude forests to hot deserts. For this, we leverage the understanding of the cellular and molecular mechanisms of temperature sensing and preference accumulated from work in the common laboratory fly *D. melanogaster*.

Thermal preference in *Drosophila* species

D. persimilis is restricted to the northern Pacific coastal range of North America, where it is found in cool forest habitats, including Dobzhansky's classic collection sites in the transition forest of the Sierra Nevada range of California, at altitudes exceeding 1,500 m (ref. 8). In line with its natural environment, in two-choice temperature preference assays, *D. persimilis* prefers distinctly cool conditions⁹ (15–20 °C; Fig. 1a,b).

D. melanogaster originated in southern Africa, from where it has colonized nearly all regions of the planet by following human migrations. Outside Africa, *D. melanogaster* is an obligate human commensal, and it is therefore perhaps not unexpected that in laboratory assays this species prefers temperatures close to those also favoured by its human host^{10,11} (about 25 °C; Fig. 1c).

D. mojavensis is endemic to the deserts of the Southwestern United States and Mexico. Deserts in this region are characteristically hot and dry, and *D. mojavensis* are exposed to extreme daily and seasonal thermal excursions, including temperatures routinely reaching above 40 °C (ref. 12), conditions that would be quickly lethal for most *Drosophila* species¹³. Again in line with their native habitat, in two-choice assays,

¹Department of Neurobiology, Northwestern University, Evanston, IL, USA. ²NSF-Simons National Institute for Theory and Mathematics in Biology, Chicago, IL, USA. ³Present address: Department of Molecular and Cell Biology, University of California, Berkeley, Berkeley, CA, USA. ⁴Present address: Department of Biology, Reed College, Portland, OR, USA. ⁵e-mail: alessia.para@northwestern.edu; marco.gallio@northwestern.edu

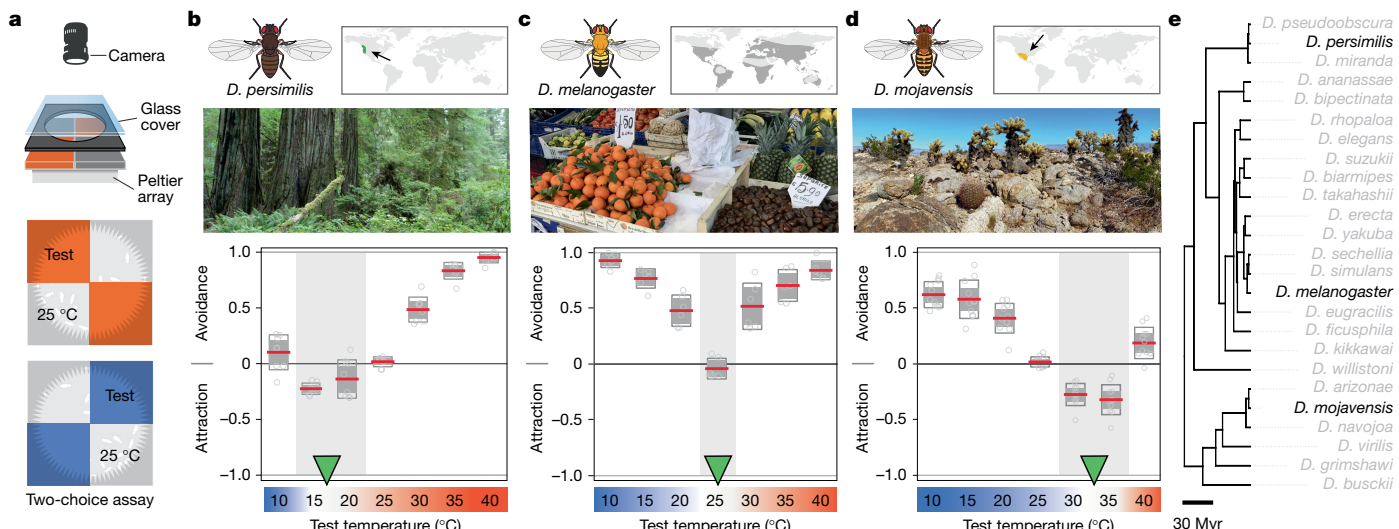


Fig. 1 | *Drosophila* species exhibit different thermal preference related to conditions in native habitats. **a**, Two-choice thermal preference assay: groups of 15 flies are given a choice between 25 °C and a variable test temperature in alternating spatial configurations; a preference index is calculated on the basis of the time spent at each temperature. **b**, *D. persimilis* is restricted to the northern Pacific coastal range of North America, where it is found in cool forest habitats. In two-choice preference assays, it prefers about 15–20 °C. **c**, *D. melanogaster* is a cosmopolitan human commensal mostly found in temperate regions and prefers about 25 °C over lower or higher temperatures.

d, *D. mojavensis* is endemic to the deserts of the southwestern United States and Mexico and prefers about 30–35 °C. In **b–d**, red lines show mean; grey boxes show one standard deviation; empty boxes show 95% confidence interval for the mean; empty circles represent data for groups of 15 flies each; $n = 8, 6$ and 11 groups per condition, respectively; grey shading shows the approximate favourite thermal range. **e**, Phylogenetic tree representing species relationships (Methods). The fly drawings in **b–d** are reproduced and adapted with permission from M. Stensmyr.

D. mojavensis prefers distinctly hot conditions^{9,14} (30–35 °C; Fig. 1d), conditions that were strongly avoided by both *D. melanogaster* and *D. persimilis*.

The three species described above hail from very different habitats and belong to groups (the *obscura*, *melanogaster* and *repleta* groups, respectively) separated by 30–50 million years¹⁵ (Fig. 1e). They therefore offer an opportunity to investigate evolutionary changes that may underlie the preference for distinct temperature ranges observed in different *Drosophila* species.

Divergent heat thresholds for Gr28b.d

In *D. melanogaster*, the preferred thermal range of about 25 °C emerges as the result of independent pushes from hot and cold avoidance, mediated by hot- and cold-sensing neurons of the antenna¹⁰. By contrast, noxious temperature responses rely on broadly tuned nociceptors found in the body¹⁶. Heat-sensing neurons of the antenna innervate the arista¹⁰ (the last antennal segment) and express the unusual ‘gustatory’ receptor molecule Gr28b.d (ref. 17). Starting from a nested set of gene promoters, the *Gr28b* locus produces five different gene products characterized by a different coding sequence, function and expression pattern (*Gr28b.a*–*Gr28b.e*; ref. 18). The Gr28b.d variant is necessary and sufficient to mediate rapid heat avoidance behaviour in the innocuous range (<35 °C (ref. 16)) and is the only variant that has proved capable of generating temperature-dependent currents in vitro¹⁹. Moreover, the sequence of Gr28b is divergent across *Drosophila* species (Fig. 2a and see Extended Data Fig. 1 for a full alignment), especially within the amino terminus and the transmembrane domains encoded by the D exon (by contrast, the pore domain is much more conserved; see Fig. 2b–d for a reconstruction and comparison between species). Gr28b.d is therefore a strong candidate innocuous-heat receptor in *Drosophila* and a prime target to test the hypothesis that differences in peripheral heat sensing may underlie species-specific differences in behaviour.

Our initial expectation was that if Gr28b.d represents the critical temperature receptor that mediates heat avoidance in *D. persimilis* and

D. mojavensis, as it does in *D. melanogaster*, the threshold of Gr28b.d heat activation in each species may reflect the onset of heat avoidance we recorded in two-choice behaviour. Our results partially support this idea (Fig. 2e–o).

First, we established an in vitro recording system (using heterologous expression in HEK293T cells and patch-clamp electrophysiology) and characterized the responses of *D. melanogaster* Gr28b.d (DmelGr28b.d; Fig. 2e–i). Our data support the notion that DmelGr28b.d is an ion channel that is activated by hot temperature¹⁹ and directly demonstrate a defined threshold for heat activation of about 26 °C (Fig. 2h and see Fig. 2n for quantification). This threshold is just above the *D. melanogaster* species-specific preferred temperature of about 25 °C (Fig. 1c) and therefore in line with the onset of behavioural heat avoidance (>25 °C). Notably, the in vitro threshold of about 26 °C was not a function of the expression system, as it was the same when DmelGr28b.d was expressed in an insect cell line (S2R+ cells from *D. melanogaster*; Fig. 2o and compare with Fig. 2n).

Next, we tested *D. persimilis* Gr28b.d (DperGr28b.d; 84% identical to the DmelGr28b.d protein sequence, Fig. 2c). In agreement with our initial hypothesis, our data showed that DperGr28b.d exhibited a lower threshold for heat activation of about 21 °C (Fig. 2j,k,n), just above the *D. persimilis* species-specific preferred range of about 15–20 °C (Fig. 1b), and again in line with the onset of behavioural heat avoidance (>20 °C).

Finally, we tested *D. mojavensis* Gr28b.d (DmojGr28b.d; 79.7% identical to DmelGr28b.d and 79.7% identical to DperGr28b.d, Fig. 2d). Notably, the threshold for heat activation of DmojGr28b.d was recorded to be about 29 °C (Fig. 2l–m), indeed higher than those of both DmelGr28b.d and DperGr28b.d (Fig. 2n). Remarkably, however, a heat activation threshold of about 29 °C would put channel opening just below the preferred *D. mojavensis* thermal range of 30–35 °C (Fig. 1d) and is therefore not in line with the onset of behavioural heat avoidance in this species (>35 °C). Rather, this observation suggests the possibility that Gr28b.d-mediated activation of hot cells may promote heat attraction in *D. mojavensis* rather than heat avoidance as it does in *D. melanogaster* and *D. persimilis*.

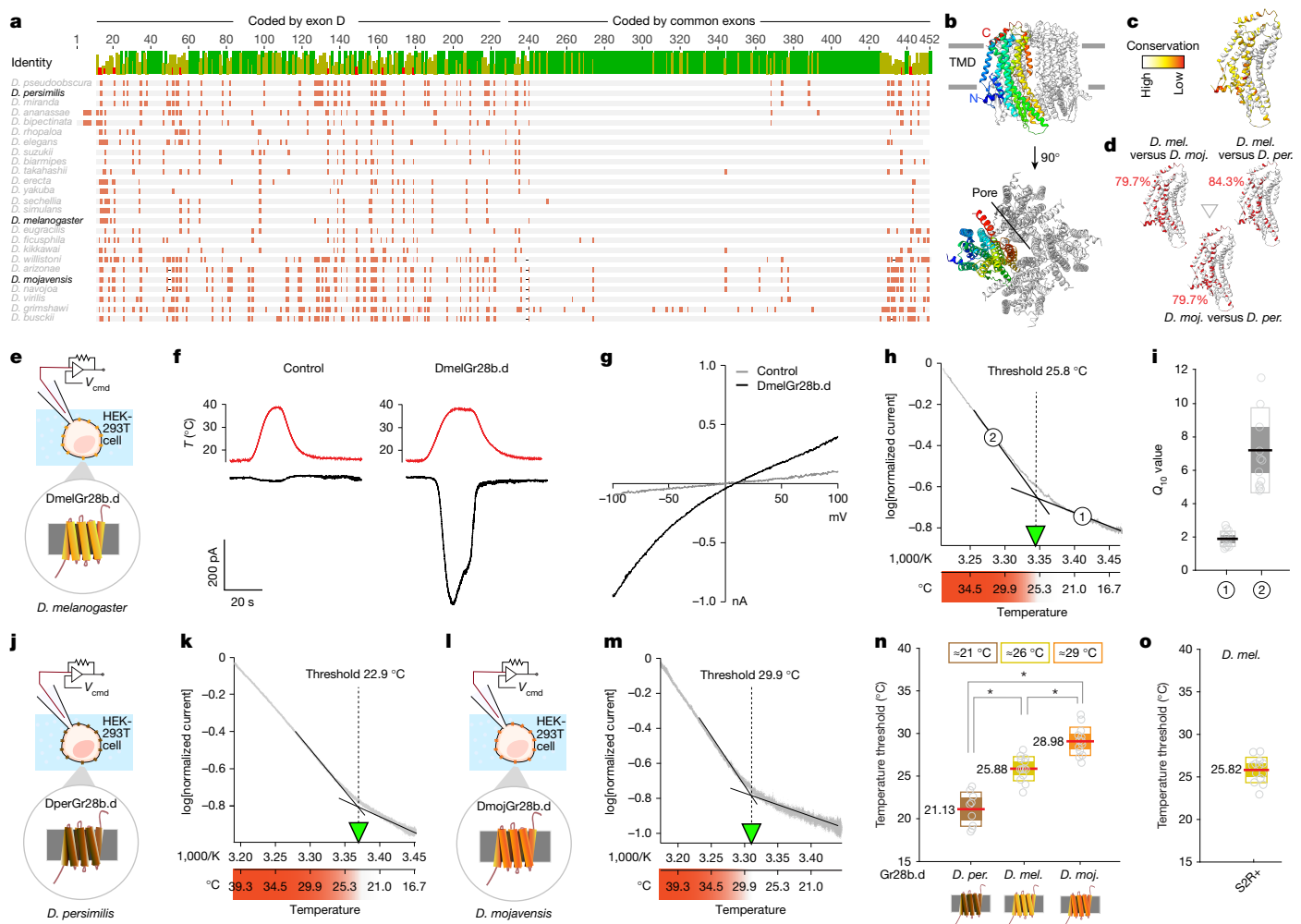


Fig. 2 | The ion channel Gr28b.d exhibits species-specific thresholds of heat activation. **a**, Gr28b.d protein alignment from 25 *Drosophila* species (histogram shows mean pairwise identity across species; green denotes 100%; red denotes <30%; orange blocks below represent variable residues). **b**, AlphaFold3 model of a Gr28b.d tetramer. TMD, transmembrane domain. **c,d**, Colour-coded conservation based on the alignment in **a** (**c**) and between the indicated species (red denotes difference, percentages are sequence identity; **d**; see also Extended Data Fig. 1). *D. mel.*, *D. melanogaster*; *D. moj.*, *D. mojavensis*; *D. per.*, *D. persimilis*. **e**, In vitro recording schematic. V_{cmd} , command voltage. **f**, Representative current-clamp recordings. Unlike control cells, cells expressing DmelGr28b.d produce an inward current in response to heating. **g**, Representative current–voltage plots from control cells (grey trace) and DmelGr28b.d-expressing cells (black trace) at about 40 °C. **h,i**, DmelGr28b.d threshold for heat activation. **h**, A representative Arrhenius plot (Methods) reveals two distinct processes characterized by different Q_{10} values; the

threshold is recorded as the intersection of the two fit lines. **i**, Q_{10} quantification ($n=13$ cells). **j,k**, Representative Arrhenius plot (**k**) from a cell expressing DperGr28b.d (**j**). **l,m**, Representative Arrhenius plot (**m**) from a cell expressing DmojGr28b.d (**l**). **n**, Systematic differences in threshold reveal species specificity ($n=9, 13$ and 13 , respectively). **o**, The threshold recorded from *Drosophila* S2R+ cells expressing DmelGr28b.d ($n=13$) is the same as that recorded in HEK293T cells (compare to **n**). In **h,k,m**, red shading denotes increasing temperature. In **i,n,o**, black lines and red lines show mean; filled boxes represent one standard deviation; empty circles represent 95% confidence interval of the mean; empty circles represent data points; each data point corresponds to one cell threshold recording; * $P<0.05$, $P=2.9\times 10^{-6}, 9.9\times 10^{-10}, 1.39\times 10^{-4}$ and 0.986 for *D. persimilis* versus *D. melanogaster*, *D. persimilis* versus *D. mojavensis*, *D. melanogaster* versus *D. mojavensis*, and *D. melanogaster* expressed in HEK293T versus in S2R+ cells, respectively; one-way analysis of variance.

Conserved heat sensing in *D. mojavensis*

D. mojavensis has evolved separately from *D. melanogaster* and *D. persimilis* for at least 30 million years, and it is therefore conceivable that their temperature-sensing system may have reconfigured, in particular when considering the unique selective pressures imposed by its extreme desert habitat. One important question is whether Gr28b.d is expressed in hot receptor neurons of the arista in *D. mojavensis* as it is in *D. melanogaster*. Our results indicate that this is the case, and that the molecular and anatomical layout of the antennal hot-sensing system is not substantially different in *D. mojavensis* as compared to *D. melanogaster* (Fig. 3a–i and see below). At the genome level, the structure of the Gr28b locus is very similar between the two species, including the existence of five predicted variants that differ in the first

coding exon, each originating from an independent gene promoter (*DmojGr28b.a–DmojGr28b.e*; Fig. 3a,b). To directly look at expression, we performed RNA sequencing of *D. mojavensis* arista samples and confirmed selective expression of the *DmojGr28b.d* variant in this organ, at levels comparable to those of other gene products that have known expression in thermoreceptors (Ir25a and Ir93a; Fig. 3c–e). We then cloned the *DmojGr28b.d* variant-specific gene promoter (by similarity with its *D. melanogaster* counterpart; Fig. 3a,b), and produced a transgenic *D. mojavensis* strain in which the Gr28b.d promoter is fused to green fluorescent protein (*Gr28b.d^{moj}-GFP*). This reagent directly allowed us to visualize expression in three neurons of the arista, which is consistent with the expression of an analogous construct in *D. melanogaster*^{10,16} and with the fact that the arista contains three hot receptor cells¹⁰ (Fig. 3f–i). Thus, our results indicate that the

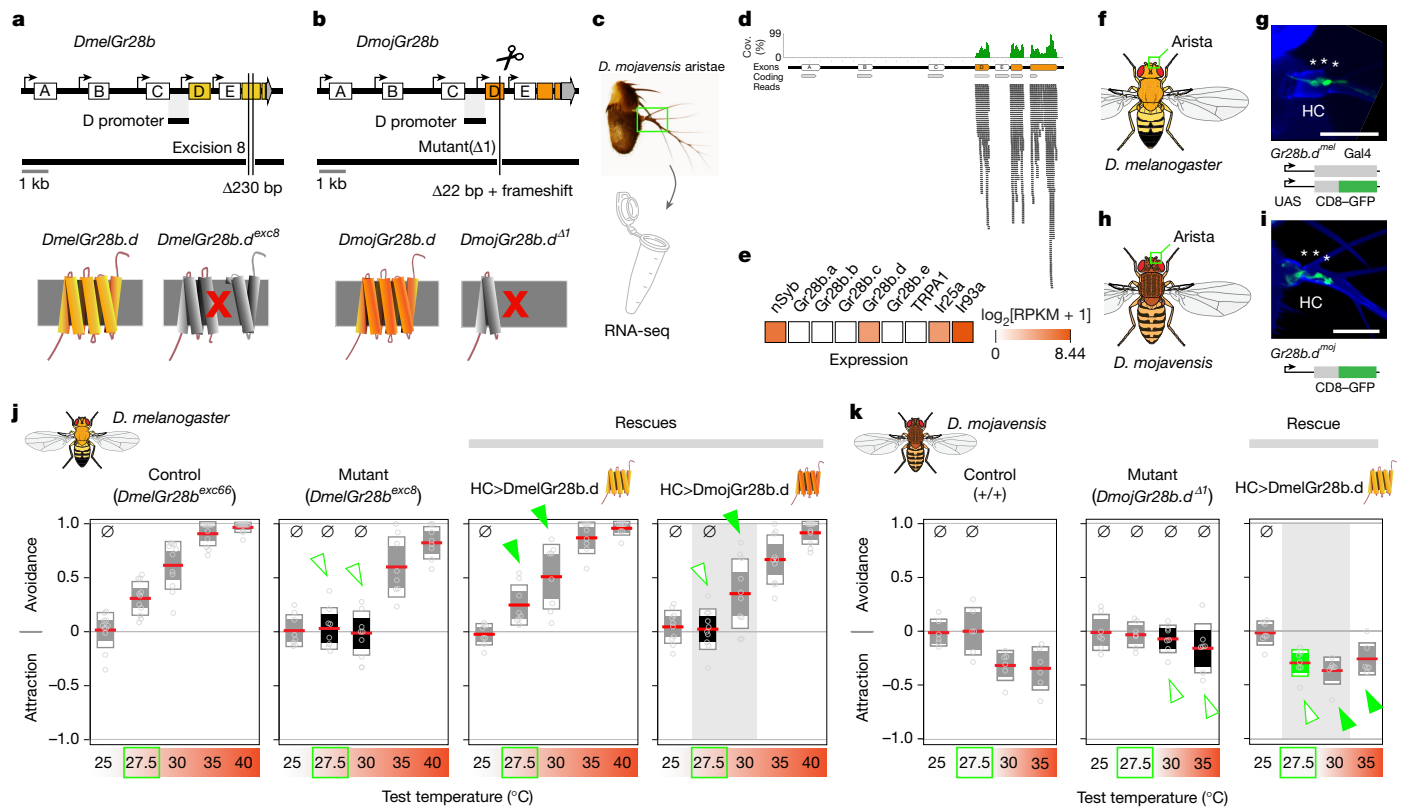


Fig. 3 | Cross-species transfer of *Gr28b.d* reveals a switch from heat avoidance to attraction in *D. mojavensis*. **a, b**, *Gr28b* genomic locus, mutations used, and their predicted effect. **a**, *DmelGr28b*. **b**, *DmojGr28b*. **c–e**, RNA sequencing (RNA-seq) of samples from *D. mojavensis* aristae demonstrates expression of the *Gr28b.d* variant. **c**, Schematic of the method. **d**, Alignment of reads to the locus. Cov., coverage. **e**, Quantification of expression; neuronal markers *nSyb*, *Ir25a* and *Ir93a* are shown for comparison. RPKM, reads per kilobase per million reads mapped. **f–i**, A *Gr28b.d* promoter fusion drives GFP expression in the three hot cells (HCs) of the arista (asterisks). **f, g**, *D. melanogaster*. **h, i**, *D. mojavensis*. **g, i**, Confocal stack of transgenics (blue: cuticle, green: GFP; scale bars, 20 μm). **j**, Control *D. melanogaster* avoid heat above 25 °C ($n = 11$ each); *DmelGr28b*^{exc8} mutants lose avoidance of 27.5 °C and 30 °C (empty arrowheads; $n = 8$ each); expression of *DmelGr28b.d* rescues avoidance starting at 27.5 °C (arrowheads; $n = 8$ each); expression of *DmojGr28b.d* rescues avoidance to 30 °C (filled arrowhead) but not 27.5 °C (empty arrowhead; $n = 10$ each). **k**, Wild-type *D. mojavensis* are indifferent to 27.5 °C but attracted to 30 °C and 35 °C

($n = 6$ each); *DmojGr28b.d*^{Δ1} mutants lose attraction to 30 °C and 35 °C (empty arrowheads; $n = 8$ each); expression of *DmelGr28b.d* in mutants rescues attraction to 30 °C and 35 °C (arrowheads) but also produces attraction to 27.5 °C (empty arrowhead; $n = 7, 7, 7$ and 6 for test temperatures from low to high). In **j, k**, two-choice, base temperature = 25 °C; red lines show mean; filled boxes show one s.d.; empty boxes show 95% confidence interval of the mean; empty circles represent data for groups, 15 flies per group; a black box and/or Ø denote not different from zero; two-tailed one-sample *t*-test, $P < 0.05$; *P* values for test temperatures from low to high are: $P = 0.331, 9.16 \times 10^{-3}, 2.21 \times 10^{-3}, 6.87 \times 10^{-7}$ and 1.11×10^{-9} for control in **j**; $P = 0.854, 0.671, 0.864, 4.94 \times 10^{-4}$ and 1.08×10^{-6} for mutant in **j**; $P = 0.331, 9.16 \times 10^{-3}, 2.21 \times 10^{-3}, 6.97 \times 10^{-7}$ and 1.11×10^{-9} for *DmelGr28b.d* rescue in **j**, and $P = 0.362, 0.685, 6.94 \times 10^{-3}, 6.49 \times 10^{-6}$ and 5.38×10^{-10} for *DmojGr28b.d* rescue in **j**; $P = 0.833, 0.986, 2.57 \times 10^{-3}$ and 8.56×10^{-3} for control in **k**; $P = 0.845, 0.443, 0.080$ and 0.282 for mutant in **k**; and $P = 0.701, 7.15 \times 10^{-4}, 2.43 \times 10^{-4}$ and 8.14×10^{-3} for *DmelGr28b.d* rescue in **k**. The fly drawings in **f, h, j, k** are reproduced and adapted with permission from M. Stensmyr.

peripheral heat-sensing mechanisms may be broadly conserved in *D. mojavensis*.

Divergent heat response in *D. mojavensis*

To directly test the possibility that *Gr28b.d*-mediated activation of the arista receptor neurons may promote heat attraction in *D. mojavensis*, rather than heat avoidance as it is known to do in *D. melanogaster*, we first compared the behavioural outcome of *Gr28b.d*-null mutations in each species. We have previously demonstrated that *DmelGr28b*-null mutants (Fig. 3a; *Gr28b.d*^{excision8} (*Gr28b.d*^{exc8}; ref. 16)) lack avoidance of innocuous heat (<35 °C) but exhibit near-normal avoidance to noxious hot temperatures (≥ 35 °C (ref. 16)), consistent with a selective role for the heat-activated arista temperature receptor neurons (TRNs) in the avoidance of innocuous heat¹⁶ (note that noxious heat responses depend instead on TRPA1, a multimodal nociceptor that is more broadly expressed^{16, 20, 21}; Fig. 3j).

Next, we produced a *DmojGr28b.d* mutant using CRISPR–Cas9 technology. Our mutant *D. mojavensis* strain carries a small deletion that is expected to result in a *Gr28b.d* truncation and is therefore a functional

channel null (*Gr28b.d*^{Δ1}; Fig. 3b and Methods). Two-choice temperature preference experiments clearly demonstrated that whereas wild-type *D. mojavensis* flies prefer 30 °C and 35 °C over 25 °C (that is, they are attracted by hot temperatures above the *D. mojavensis* species-specific threshold of *Gr28b.d* activation, about 29 °C), *DmojGr28b.d*^{Δ1} mutants lack attraction to 30 °C and 35 °C and spend equal time at those temperatures as compared to 25 °C (Fig. 3k; and note that the *DmojGr28b.d*^{Δ1} mutant exhibited normal avoidance of ‘noxious’ heat >40 °C; Extended Data Fig. 2).

Together, our results support the notion that, in both *D. melanogaster* and *D. mojavensis*, *Gr28b.d* (and the TRNs of the arista that express it) selectively mediates the responses to innocuous heat. Moreover, the phenotype of the mutants clearly demonstrates that whereas activation of *Gr28b.d* mediates innocuous-heat avoidance in *D. melanogaster*, it mediates innocuous-heat attraction in *D. mojavensis*.

Cross-species rescue of *Gr28b.d*

If *Gr28b.d* mediates activation of the hot receptor neurons in both *D. melanogaster* and *D. mojavensis*, and if that results in opposing

behaviour in each species (heat attraction in *D. mojavensis* and avoidance in *D. melanogaster*), cross-species rescue should reinstate the appropriate species-specific behaviour of the host species (avoidance for *D. melanogaster* and attraction for *D. mojavensis*). Furthermore, if the species-specific threshold of activation of Gr28b.d in vitro reflects its properties in vivo, cross-species rescue would be expected to impart the threshold of activation of the donor species.

Our results confirm these hypotheses (Fig. 3j,k). Here our goal was to perform a cross-species swap of the Gr28b.d receptor (that is, a transgenic rescue of a *Gr28b* mutant in each of the two species using a coding sequence from the other). First, we used the *Gr28b*-null mutant (*Gr28b*^{exc8} (ref. 16)) and attempted to rescue its heat avoidance phenotype using a *DmojGr28b.d* construct.

We have previously shown that expression of the endogenous *DmelGr28b.d* variant in hot cells of the arista can fully rescue the avoidance of 30 °C (innocuous heat) in *D. melanogaster* *DmelGr28b*^{exc8}-null mutants¹⁶. To test for cross-species rescue, we used again our two-choice assay (and 25 °C as a base temperature; Fig. 1) and used a set of test temperatures in the hot range spanning the activation threshold we recorded in vitro for *DmelGr28b.d* (about 26 °C) and *DmojGr28b.d* (about 29 °C). Our data demonstrate that same-species rescue restores the normal *D. melanogaster* avoidance of hot temperatures starting at 27.5 °C, in line with the in vitro activation threshold of *DmelGr28b.d* of about 26 °C. Notably, expression of *DmojGr28b.d* in *D. melanogaster* mutant flies also restored avoidance, but only to 30 °C and not to 27.5 °C, which is consistent with the *DmojGr28b.d* activation threshold of about 29 °C we recorded in vitro (Fig. 3j). Hence, expression of *DmojGr28b.d* in *D. melanogaster* mutant flies restores normal heat avoidance to the mutant but with a *D. mojavensis*-like threshold (about 30 °C).

Our next goal was to perform the reciprocal experiment (that is, to rescue the behavioural phenotype of the *DmojGr28b.d* mutant using a *DmelGr28b.d* construct). Indeed, our two-choice experiments confirmed that wild-type *D. mojavensis* flies are indifferent to 27.5 °C but prefer 30 °C and 35 °C over 25 °C (that is, they are attracted by hot temperatures above the threshold of *DmojGr28b.d* activation (about 29 °C)). As expected, *DmojGr28b.d*^{d1} mutants lacked attraction to 27.5 °C, but also to 30 °C and 35 °C, and spent equal amounts of time at those temperatures as compared to 25 °C (Fig. 3k). Finally, we engineered a cross-species transgenic rescue, by fusing the *DmojGr28b.d* variant-specific promoter to a *DmelGr28b.d*-coding sequence, and stably transformed this construct into a *D. mojavensis* strain that is also a *Gr28b.d*^{d1} homozygous mutant (Fig. 3k and Methods). Cross-species rescue of *DmojGr28b.d*^{d1} flies using the *D. melanogaster* construct restored heat attraction in the mutant. Remarkably, the *D. melanogaster*-rescued *D. mojavensis* now seemed to also be attracted to 27.5 °C, a temperature that their wild-type counterpart were indifferent to. The temperature 27.5 °C is below the normal threshold for activation of the *D. mojavensis* channel (about 29 °C) but above the normal threshold for activation of the *D. melanogaster* channel (about 26 °C). We conclude that the cross-species rescue restored behavioural heat attraction in the *D. mojavensis* mutant, but now imparted a *D. melanogaster*-like threshold to behaviour.

Mapping heat pathways in *D. mojavensis*

Our results demonstrate that Gr28b.d-mediated activation of hot receptor cells results in opposite behaviour in *D. melanogaster* (heat avoidance), compared with that of *D. mojavensis* (heat attraction). This implies that the valence of heat stimuli (below the noxious range) has switched from aversive to attractive in the desert species, and that the central thermosensory system must be wired differently in *D. mojavensis*.

To explore this possibility, our next goal was to reconstruct the neuronal pathways that relay temperature signals in the brain of *D. mojavensis* and compare them with their well-known counterparts in

D. melanogaster^{22–24} (Fig. 4). First, we used our transgenic *D. mojavensis* flies in which a *Gr28b.d* promoter fusion labels the three hot receptor neurons of the arista (see above) and imaged the brain to visualize their projections in the posterior antennal lobe (PAL; see Fig. 4a,b for a schematic of the cells and brain regions involved). Our results demonstrate that, in *D. mojavensis*, hot receptors of the arista target a location in the PAL similar to the ‘hot glomerulus’ targeted by the analogous hot receptor cells in *D. melanogaster*^{10,22} (Fig. 4b,c).

Next we turned our attention to the second-order neurons of the thermosensory system: the thermosensory projection neurons (TPNs), cells that are directly postsynaptic to the antennal receptors (TRNs) and that extend axons to innervate higher brain centres. We and others have previously characterized TPN pathways in *D. melanogaster* in detail^{22–24} (Fig. 4d). In fact, owing to the stereotypy of the fly brain, the same cells and cell types can be recognized from fly to fly and between electron microscopy (EM) and light microscopy reconstructions²⁵. The TPNs represent the main conduit for the relay of thermosensory signals to regions of the brain that process both innate and learned behaviour (such as the lateral horn (LH) and mushroom body, respectively), and are therefore uniquely positioned as a potential substrate for the evolutionary rewiring of heat signals from avoidance into attraction.

Here our goal was to label specific TPN cell types in the brain of *D. mojavensis*, study their anatomy, and compare their organization to that of *D. melanogaster* TPNs. For this, we again turned to our *Gr28b.d*^{moj}-GFP transgenics and, using GFP fluorescence as a guide, targeted a dye-filled electrode into the brain and to the hot glomerulus of the PAL: a brief electrical shock resulted in stochastic dye labelling of one to a few TPNs innervating the hot glomerulus (Extended Data Fig. 3a and Methods).

Dye labelling revealed that the main TPN pathways that we previously described in *D. melanogaster* are also present in *D. mojavensis*, so that the same cell types we described in light microscopy (and later reconstructed in the EM connectome) of *D. melanogaster* could be identified in dye fills of this species. These include, for example, projection neurons that innervate both the hot and cold glomerulus of the PAL (TPN-Ia, TPN-Ib, TPN-III and TPN-VI; Fig. 4e). In fact, for *D. melanogaster*, the frequency of dye labelling of each TPN cell type corresponded well with the degree of connectivity with the TRNs innervating the hot glomerulus (Fig. 4f and Extended Data Fig. 4a) and was very similar to that observed in *D. mojavensis* (and in the other species described below; Extended Data Fig. 4b–d). Hence, the overall organization of TPN pathways seems conserved between *D. melanogaster* and *D. mojavensis*.

Divergent TPN-V innervation of the LH

To explore the connectivity of Gr28b.d-expressing cells to higher brain centres, we focused our attention on the TPN cell type that, according to connectomic analysis in *D. melanogaster*, represents the main common TPN synaptic output of the hot receptors of the arista: a cell type that we previously described as TPN-V (ref. 26; receiving 26% of the combined output synapses of the three arista hot TRNs; Fig. 4f and Methods). Consistent with its privileged connectivity with the hot cells, TPN-V was by far the most common TPN cell type labelled in our experiments (28/32 brains we injected had at least some TPN-V labelling; Extended Data Fig. 4). As expected, TPN-V dye fills in *D. melanogaster* showed innervation of the calyx of the mushroom body²⁶ (especially of the lateral accessory calyx (IACA) Fig. 4h,h', asterisk) as well as of the ventral region of the LH (Fig. 4i,i', arrowheads). Again as expected, the TPN-V pattern of innervation highlighted in our dye fill experiments in *D. melanogaster* was highly consistent across individuals and with EM reconstructions.

Notably, *D. mojavensis* TPN-V demonstrated a distinct pattern of innervation both in the IACA of the mushroom body and in the LH (Fig. 4h,i). First, in *D. mojavensis*, the innervation of the IACA by TPN-V appeared more extensive than that of *D. melanogaster* (asterisks in

Article

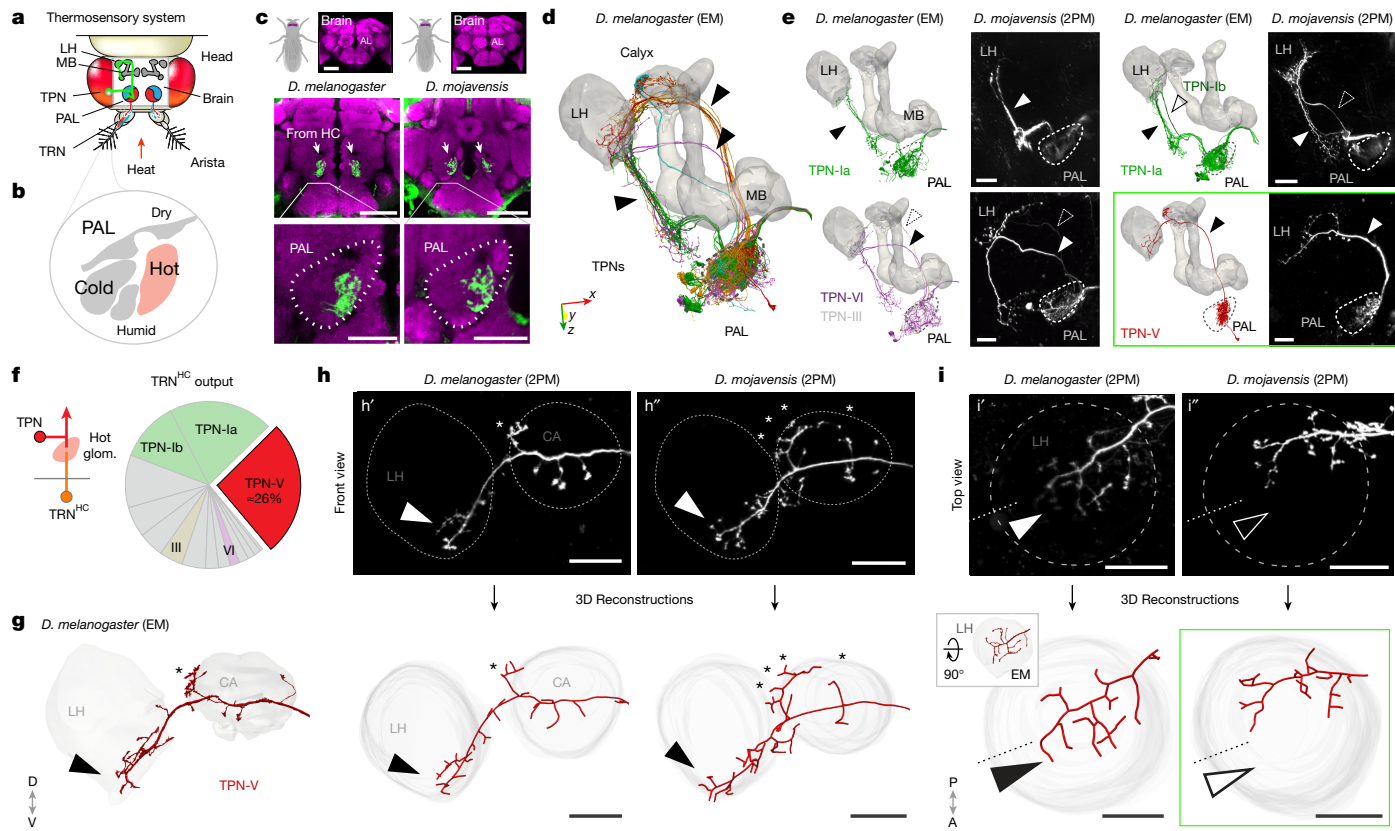


Fig. 4 | Differential morphology of central pathways that relay heat signals in the *D. mojavensis* brain. **a**, Thermosensory cell types. **b**, PAL glomeruli. **c**, Confocal stacks from *D. melanogaster* (left) and *D. mojavensis* (right) brains stained by the neuropil marker nc82 (magenta). Below, the axon terminals of hot-activated TRN of the antenna are independently labelled by transgenic expression of GFP (stained by anti-GFP, green; arrows). AL, antennal lobe. Scale bars, 50 μ m. **d**, EM reconstruction of TPN pathways in *D. melanogaster*; front view. MB, mushroom body. **e**, *D. melanogaster* EM reconstructions paired with representative two-photon microscopy (2PM) images of similar dye-labelled *D. mojavensis* TPNs. Cell types: TPN-Ia, TPN-Ib, TPN-VI and TPN-V (arrowheads); empty arrowheads mark additional pathways. Scale bars, 25 μ m. Dye fill statistics are provided in Extended Data Fig. 4. **f**, Schematic of cell types involved and pie chart of the common TPN synaptic output of hot-activated TRNs. Glom., glomerulus. **g**, EM reconstruction of *D. melanogaster* TPN-V showing innervation

of the IACA (asterisk) and ventral LH (arrowhead; front view shows anterior-posterior axis). CA, calyx; D, dorsal; V, ventral. **h,i**, Representative two-photon z-stacks of dye-labelled TPN-V, in *D. melanogaster* (**h',i'**) and *D. mojavensis* (**h'',i''**). **h**, front view. In *D. mojavensis*, TPN-V more densely innervates the IACA, as compared to *D. melanogaster* (asterisks). In both cases, TPN-V veers to innervate the ventral aspect of the LH (arrowheads). **i**, Top view. Two-photon stacks demonstrate a broader innervation within the anterior–ventral LH in *D. melanogaster* (**i'**, arrowheads) compared with *D. mojavensis* (**i''**, empty arrowheads). Bottom panels in **h** and **i** are 3D reconstructions of the dye-filled neurons (Methods), the small inset in **i** is an EM reconstruction shown for comparison. P, posterior; A, anterior. Scale bars, 25 μ m. Dashed lines in **h,i** outline the calyx and LH; dotted line is for reference across panels. Green outlines are included for emphasis.

Fig. 4h'' and compare with Fig. 4h'); second, TPN-V innervation of the LH followed a different pattern in *D. mojavensis* as compared to *D. melanogaster*. In *D. melanogaster*, TPN-V axons form en passant synapses within the calyx; they then veer ventrally to invade the LH (Fig. 4h,h', arrowheads). A dorsal view illustrates how the *D. melanogaster* TPN-V axon innervates the LH along its diameter and arborizes extensively extending branches towards both the anterior and posterior LH region (Fig. 4i,i'). *D. mojavensis* TPN-V also veers ventrally to innervate the LH (Fig. 4h'', arrowheads). Yet, in contrast to their *D. melanogaster* counterpart, TPN-V projections within the ventral LH appear less extensive and are limited to the posterior half of the ventral LH region. In fact, in *D. mojavensis*, the anterior–ventral LH appears to entirely lack TPN-V innervation (Fig. 4i'', empty arrowheads, and compare with Fig. 4i', arrowheads; and Extended Data Fig. 3 and see Methods for details on reconstructions).

Although a different pattern of TPN-VIACA innervation in the two species may reflect a number of differences in temperature processing and behaviour (for example, in temperature regulation of sleep^{26,27}), differential innervation of the LH is potentially very important in the context of innate heat attraction or avoidance, as the LH has previously been

implicated as a key centre for the processing of olfactory valence^{1–5}. Hence, at face value, our results indicate that differential TPN-V innervation of the LH in *D. melanogaster* versus *D. mojavensis* may reflect differential wiring of thermosensory projections in this region, which in turn could explain the switch from heat avoidance to attraction.

In support of this idea, in *D. melanogaster*, TPN-V projections within the ventral LH target at least two cell types whose normal activity is essential for heat avoidance: the thermosensory LH output neuron I (TLHON-I), a cell type we recently identified as involved in rapid heat avoidance²⁸; and TLHON-II, a cell type we report here as the main synaptic output of TPN-V (both overall and within the LH; Extended Data Fig. 5a–c and Methods). We identify a driver exclusively active in this cell type (Extended Data Fig. 5) and show that genetic silencing of TLHON-II severely reduces heat avoidance, whereas optogenetic activation triggers avoidance of the optogenetic stimulus (Extended Data Fig. 5d–f). Hence, in *D. melanogaster*, the targets of TPN-V in the LH (TLHON-I and TLHON-II, in particular) are critical to process the aversive valence of heat.

As *D. melanogaster* and *D. mojavensis* have evolved separately for about 50 million years and belong to different *Drosophila* groups, the

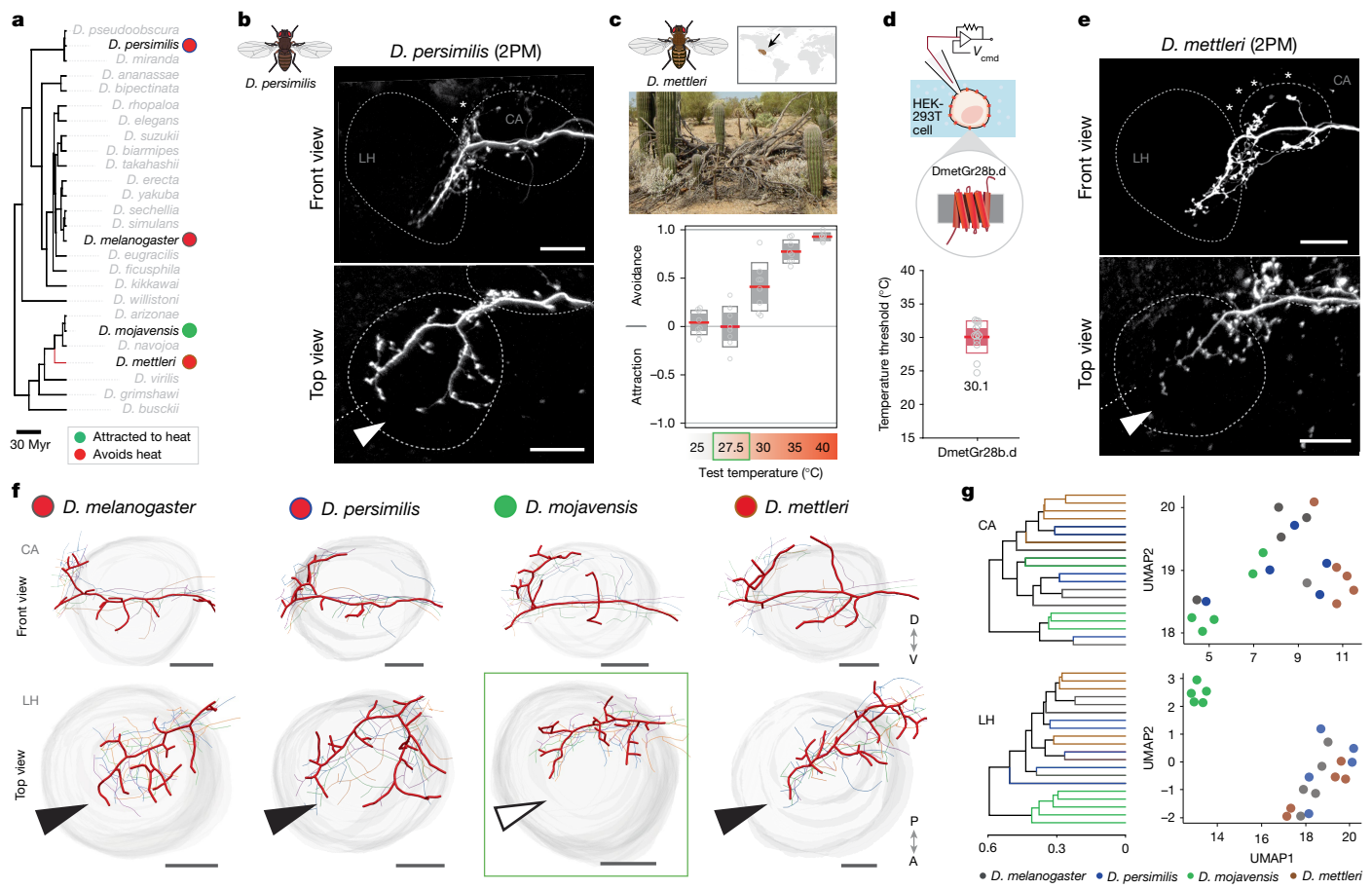


Fig. 5 | TPN-V innervation of the LH matches behaviour rather than following phylogeny. **a**, Phylogenetic tree. **b**, Representative two-photon z-stacks of dye-labelled TPN-V terminals in the calyx and LH of *D. persimilis*; upper panel: front view (z-projection of a scan acquired on the anterior–posterior axis), illustrating innervation of the calyx (IACA, asterisks); lower panel: top view (z-projection of a scan acquired on the dorsal–ventral axis), illustrating innervation of the anterior–ventral LH (arrowhead). **c**, *D. mettleri* avoids heat above 27.5 °C in two-choice assays. **d**, The in vitro threshold for heat activation of *D. mettleri* Gr28b.d is about 30 °C. In **c,d**, red lines show mean; filled boxes show one standard deviation; empty boxes show 95% confidence interval of the mean; empty circles represent data points; in **c**, $n = 8$ groups of 15 flies; in **d**, $n = 13$ recordings. **e**, Representative two-photon z-stacks of TPN-V terminals in the calyx and LH of *D. mettleri* (upper panel: front view; lower panel: top view;

in **b,e**, dashed ovals outline the calyx and LH; dotted line is for reference). **f**, 3D reconstructions of TPN-V arboretions from *D. melanogaster*, *D. persimilis*, *D. mojavensis* and *D. mettleri*, respectively ($n = 5$ each, aligned within species; Methods). In top views, the LH innervation of the *D. mojavensis* TPN-V stands out as lacking any projections in the anterior–ventral LH (empty arrowhead). **g**, A distance matrix for reconstructions in **f** (Methods) demonstrates distinct clustering of the *D. mojavensis* TPN-V arboretions within the LH. Cell–cell distances are represented both as a dendrogram (left) and UMAP (clustering P value = 1.97×10^{-5} , SigClust test). In **g**, every dendrogram line or UMAP dot represents a reconstruction in **f**. In **a,f**, red and green dots denote heat avoidance and attraction, respectively. In **g**, colour represents species. Scale bars, 25 μm (**b,e,f**). The fly drawings in **b,c** are reproduced and adapted with permission from M. Stensmyr.

different pattern of TPN-V LH innervation may reflect lineage-specific differences in LH architecture rather than selective differences in its innervation by TPNs that relay heat. To explore this possibility, as an ‘internal control’, we reconstructed a well-characterized olfactory projection neuron pathway that innervates the LH in both *D. melanogaster* and *D. mojavensis* (using two-colour two-photon microscopy in the same *D. mojavensis* brain; Extended Data Fig. 6). Our results directly demonstrate that the LH architecture of *D. mojavensis* is not very different from that of *D. melanogaster* (in fact, the olfactory projections we map are very similar between the two species; Extended Data Fig. 6), supporting the notion that a different pattern of innervation of the LH by TPN-V in *D. mojavensis* may reflect differential wiring to TLHONs and correlate with the change in behaviour we observe.

LH innervation matches species behaviour

Our next goal was to extend these results and to rule out the possibility that, in *Drosophila* species, the pattern of LH innervation may follow a species’ phylogenetic relationships rather than matching temperature

preference behaviour (Fig. 5a). For this, we devised a strategy that allowed us to target the hot glomerulus of the PAL and to dye-label TPN-V by in vivo electroporation without resorting to transgenic reagents: we loaded the arista nerve (containing the axons of TRNs innervating the hot and cold glomerulus of the PAL) with a red fluorescent dye; then we dissected the brain and, under a two-photon microscope, targeted the hot glomerulus of the PAL for electroporation as before.

First, we directed our attention to *D. persimilis*, a species that in our experiments preferred distinctly cooler conditions than *D. melanogaster* (15–20 °C) and that robustly avoided temperatures above this range, with a matching threshold for Gr28b.d heat activation (about 21 °C, see above; Fig. 2k,n). Notably, the *D. persimilis* TPN-V innervation pattern was similar to that of *D. melanogaster* within both the mushroom body and the ventral LH (Fig. 5b). Innervation of the IACA appeared more pronounced than in *D. melanogaster* (asterisks). Our dye fills demonstrated substantial innervation of the anterior–ventral LH in *D. persimilis*, similar to what we described for *D. melanogaster* (Fig. 5b, top view, arrowhead) and again supporting a correlation between innervation of the anterior–ventral LH and heat avoidance. We also tested one

Article

additional strain each of *D. melanogaster*, *D. mojavensis* and *D. persimilis* (chosen, when possible, to represent a distinct origin within the geographic range of each species). Our results demonstrate the stability of the correlation of thermal preference behaviour and TPN-V innervation patterns between strains of the same species (Extended Data Fig. 7).

Next, we focused on *D. mettleri*, a desert relative of *D. mojavensis* that has the unusual distinction of having the lowest heat tolerance among the four *Drosophila* species endemic to the desert²⁹, a trait that is believed to relate to its unique ability to breed in the cooler soil moistened by liquid excreted by rotting cacti (rather than on the cacti themselves¹²). In our two-choice assays, *D. mettleri* demonstrated clear heat avoidance, both in the innocuous and noxious range (Fig. 5c). Despite its phylogenetic relationship with *D. mojavensis*, the fact that *D. mettleri* avoids heat (rather than being attracted to it like *D. mojavensis*) creates an ideal natural experiment, as this species is closer to *D. mojavensis* by descent, but more similar to *D. melanogaster* and *D. persimilis* in temperature preference behaviour (heat avoidance). Notably, in two-choice assays, this species seems indifferent to 27.5 °C (like *D. mojavensis*) but robustly avoids 30 °C (like *D. melanogaster*); if indeed the threshold of activation of Gr28b.d determines the threshold of the specific response to heat, one would predict a threshold between 27.5 °C and 30 °C for the *D. mettleri* channel. This is very close to the threshold we recorded in vitro (about 30 °C, Fig. 5d, and see Extended Data Fig. 1b for an alignment of the channels), demonstrating that receptor threshold and behavioural outcome (attraction/avoidance) can be separated even in the same group of species (the *repleta* group, to which both *D. mojavensis* and *D. mettleri* belong).

Finally, we performed dye fills in the *D. mettleri* brain. Our results show ample TPN-V innervation of the anterior–ventral LH in this species (Fig. 5e), more closely resembling the innervation pattern of *D. melanogaster* and *D. persimilis* than that of its relative *D. mojavensis* (see Fig. 5f for side-by-side three-dimensional (3D) reconstructions). By contrast, the *D. mettleri* pattern of TPN-V innervation within the IACA appears to lie in between that of *D. mojavensis* and *D. persimilis* (Fig. 5e,f, asterisks). To better quantify these differences in innervation, we developed a pipeline that allows one to align 3D reconstructions of dye-filled neurites within species (Fig. 5f, using the volume of the LH and calyx as a guide) and to compare branching morphologies and innervation patterns across species (combining distances in morphology space calculated by CAJAL³⁰ with a measure of centre of mass for each neuron's innervation; Extended Data Fig. 3 and Methods). The cell–cell distances obtained are then used to produce a dendrogram and to represent clustering in uniform manifold approximation and projection (UMAP; Fig. 5g) space. The results of this analysis show that the *D. mojavensis* TPN-V innervation of the LH indeed stands out as different from that of the other species.

Taken together, our results support the idea that the pattern of TPN-V innervation within the anterior–ventral LH correlates with temperature preference behaviour (heat avoidance or attraction) rather than phylogeny in each of the four *Drosophila* species (Fig. 5f). Moreover, our results support a model in which the ventral LH may be a key substrate for the evolutionary switch from heat avoidance into heat attraction we describe in the brain of the desert-dwelling *D. mojavensis*.

Discussion

Despite the critical role of temperature in shaping the distribution of animal species, we know little on how animals adapt to different thermal conditions during the colonization of new environments. One open question is whether, like for the olfactory and taste systems (for example, refs. 31–33), thermal preference behaviour can evolve directly as a result of changes in the response properties of peripheral sensory neurons and of the molecular receptors they express. Recent work has led to the discovery of many of the molecular mechanisms that endow thermosensory neurons with the ability to respond

to changes in external temperature, and in some cases the *in vitro* properties of the ion channels that function as molecular receptors in different animal species broadly correlate with the overall thermal range of their habitat. Yet the observed differences in channel properties have been so far linked to differences in thermal tolerance rather than thermal preference^{34,35}. For example, the heat receptor TRPV1 of ground squirrels and camels has lower overall sensitivity to heat than the homologous receptors from rat or humans, an adaptation that has been suggested to relate to the higher heat tolerance of this species³⁴. We do not know whether specific changes in the activation threshold of hot and cold receptor molecules may also represent an evolutionary mechanism to shift a species' behavioural preference towards a different thermal niche.

Here, using species of the genus *Drosophila* adapted to life in diverse thermal environments, we show that ecologically relevant shifts in thermal preference can be explained by changes in the activation threshold of the innocuous-heat receptor Gr28b.d (as we demonstrate for *D. melanogaster* and *D. persimilis*). Unexpectedly, whereas Gr28b.d activation results in heat avoidance in both *D. melanogaster* and *D. persimilis*, adaptation to desert life in *D. mojavensis* seems to have required a substantial additional change, as Gr28b.d-mediated activation of hot-sensing neurons in this species results in innocuous-heat attraction rather than avoidance. Our data further indicate that this change may involve central thermosensory circuits within the ventral LH, a region of the fly brain historically associated with processing innate behaviours and sensory valence^{1–5}.

The benefit of such a marked change in behaviour in the context of adaptation to the desert climate is not obvious. In the cosmopolitan *D. melanogaster*, the preferred thermal range emerges as the result of opposing pushes from hot and cold avoidance¹⁰, so that, in permissive conditions, the thermosensory system is less active (which is energetically less costly). The microclimate that *D. mojavensis* experience has been studied in detail in the Sonoran Desert of southwestern North America: habitat temperatures often exceed even the very high thermal tolerance limits for this species, and flies in the field are exposed to highly variable temperatures, sometimes ranging between <5 °C to >40 °C in a single 24-h period¹². We speculate that heat attraction may have originated in the *D. mojavensis* lineage as a response to the extreme thermal excursions that flies encounter on a daily basis in their desert habitat. In such conditions, tracking temperature changes and seeking out suitable thermal niches may represent a constant priority.

How behaviour evolves to support adaptation to new environmental conditions is a central question in evolutionary biology. Our results advance our knowledge on the evolution of temperature preference in *Drosophila* species, establish a framework for studying the neurobiological determinants of thermal habitat preference in the insects, and may eventually help us better understand the impact of climate change on the distribution of invertebrates and on the many systems that depend on them.

Online content

Any methods, additional references, Nature Portfolio reporting summaries, source data, extended data, supplementary information, acknowledgements, peer review information; details of author contributions and competing interests; and statements of data and code availability are available at <https://doi.org/10.1038/s41586-025-08682-z>.

1. Das Chakraborty, S., Chang, H., Hansson, B. S. & Sachse, S. Higher-order olfactory neurons in the lateral horn support odor valence and odor identity coding in *Drosophila*. *eLife* **11**, e74637 (2022).
2. Frechter, S. et al. Functional and anatomical specificity in a higher olfactory centre. *eLife* **8**, e44590 (2019).
3. Knaden, M., Strutz, A., Ahsan, J., Sachse, S. & Hansson, B. S. Spatial representation of odorant valence in an insect brain. *Cell Rep.* **1**, 392–399 (2012).

4. Lerner, H., Rozenfeld, E., Rozenman, B., Huetteroth, W. & Parnas, M. Differential role for a defined lateral horn neuron subset in naïve odor valence in *Drosophila*. *Sci. Rep.* **10**, 6147 (2020).
5. Varela, N., Gaspar, M., Dias, S. & Vasconcelos, M. L. Avoidance response to CO₂ in the lateral horn. *PLoS Biol.* **17**, e2006749 (2019).
6. Sinervo, B. et al. Erosion of lizard diversity by climate change and altered thermal niches. *Science* **328**, 894–899 (2010).
7. Warren, M. S. et al. The decline of butterflies in Europe: problems, significance, and possible solutions. *Proc. Natl Acad. Sci. USA* <https://doi.org/10.1073/pnas.2002551117> (2021).
8. Contributions to the genetics, taxonomy, and ecology of *Drosophila pseudoobscura* and its relatives. *Ann. Entomol. Soc. Am.* **39**, 151 (1946).
9. Ito, F. & Awasaki, T. Comparative analysis of temperature preference behavior and effects of temperature on daily behavior in 11 *Drosophila* species. *Sci. Rep.* **12**, 12692 (2022).
10. Gallio, M., Ofstad, T. A., Macpherson, L. J., Wang, J. W. & Zuker, C. S. The coding of temperature in the *Drosophila* brain. *Cell* **144**, 614–624 (2011).
11. Sayeed, O. & Benzer, S. Behavioral genetics of thermosensation and hygrosensation in *Drosophila*. *Proc. Natl Acad. Sci. USA* **93**, 6079–6084 (1996).
12. Gibbs, A. G., Perkins, M. C. & Markow, T. A. No place to hide: microclimates of Sonoran Desert *Drosophila*. *J. Therm. Biol.* **28**, 353–362 (2003).
13. Kellermann, V. et al. Upper thermal limits of *Drosophila* are linked to species distributions and strongly constrained phylogenetically. *Proc. Natl Acad. Sci. USA* **109**, 16228–16233 (2012).
14. Huda, A., Omelchenko, A. A., Vaden, T. J., Castaneda, A. N. & Ni, L. Responses of different *Drosophila* species to temperature changes. *J. Exp. Biol.* <https://doi.org/10.1242/jeb.243708> (2022).
15. Suvorov, A. et al. Widespread introgression across a phylogeny of 155 *Drosophila* genomes. *Curr. Biol.* **32**, 111–123 (2022).
16. Simoes, J. M. et al. Robustness and plasticity in *Drosophila* heat avoidance. *Nat. Commun.* **12**, 2044 (2021).
17. Ni, L. et al. A gustatory receptor parologue controls rapid warmth avoidance in *Drosophila*. *Nature* **500**, 580–584 (2013).
18. Thorne, N. & Amrein, H. Atypical expression of *Drosophila* gustatory receptor genes in sensory and central neurons. *J. Comp. Neurol.* **506**, 548–568 (2008).
19. Mishra, A. et al. The *Drosophila* Gr28bD product is a non-specific cation channel that can be used as a novel thermogenetic tool. *Sci. Rep.* **8**, 901 (2018).
20. Arenas, O. M. et al. Activation of planarian TRPA1 by reactive oxygen species reveals a conserved mechanism for animal nociception. *Nat. Neurosci.* **20**, 1686–1693 (2017).
21. Hamada, F. N. et al. An internal thermal sensor controlling temperature preference in *Drosophila*. *Nature* **454**, 217–220 (2008).
22. Frank, D. D., Jouandet, G. C., Kearney, P. J., Macpherson, L. J. & Gallio, M. Temperature representation in the *Drosophila* brain. *Nature* **519**, 358–361 (2015).
23. Liu, W. W., Mazor, O. & Wilson, R. I. Thermosensory processing in the *Drosophila* brain. *Nature* **519**, 353–357 (2015).
24. Marin, E. C. et al. Connectomics analysis reveals first-, second-, and third-order thermosensory and hygrosensory neurons in the adult *Drosophila* brain. *Curr. Biol.* **30**, 3167–3182 (2020).
25. Schlegel, P. et al. Whole-brain annotation and multi-connectome cell typing of *Drosophila*. *Nature* **634**, 139–152 (2024).
26. Alpert, M. H., Gil, H., Para, A. & Gallio, M. A thermometer circuit for hot temperature adjusts *Drosophila* behavior to persistent heat. *Curr. Biol.* **32**, 4079–4087 (2022).
27. Alpert, M. H. et al. A circuit encoding absolute cold temperature in *Drosophila*. *Curr. Biol.* **30**, 2275–2288 (2020).
28. Jouandet, G. C. et al. Rapid threat assessment in the *Drosophila* thermosensory system. *Nat. Commun.* **14**, 7067 (2023).
29. Stratman, R. & Markow, T. A. Resistance to thermal stress in desert *Drosophila*. *Funct. Ecol.* **12**, 965–970 (1998).
30. Govek, K. W. et al. CAJAL enables analysis and integration of single-cell morphological data using metric geometry. *Nat. Commun.* **14**, 3672 (2023).
31. Auer, T. O. et al. Olfactory receptor and circuit evolution promote host specialization. *Nature* **579**, 402–408 (2020).
32. Stensmyr, M. C., Dekker, T. & Hansson, B. S. Evolution of the olfactory code in the *Drosophila melanogaster* subgroup. *Proc. Biol. Sci.* **270**, 2333–2340 (2003).
33. Toda, Y. et al. Early origin of sweet perception in the songbird radiation. *Science* **373**, 226–231 (2021).
34. Laursen, W. J., Schneider, E. R., Merriman, D. K., Bagriantsev, S. N. & Gracheva, E. O. Low-cost functional plasticity of TRPV1 supports heat tolerance in squirrels and camels. *Proc. Natl Acad. Sci. USA* **113**, 11342–11347 (2016).
35. Yang, S. et al. A paradigm of thermal adaptation in penguins and elephants by tuning cold activation in TRPM8. *Proc. Natl Acad. Sci. USA* **117**, 8633–8638 (2020).

Publisher's note Springer Nature remains neutral with regard to jurisdictional claims in published maps and institutional affiliations.

Springer Nature or its licensor (e.g. a society or other partner) holds exclusive rights to this article under a publishing agreement with the author(s) or other rightsholder(s); author self-archiving of the accepted manuscript version of this article is solely governed by the terms of such publishing agreement and applicable law.

© The Author(s), under exclusive licence to Springer Nature Limited 2025

Methods

Fly stocks and husbandry

All *Drosophila* strains were reared on cornmeal agar medium at room temperature (about 23 °C). *D. melanogaster* fly stocks and sources are as follows: Canton-S, HC>Gal4 (ref. 10), HC>LexA (ref. 22), Gr28b.d(exc66) and Gr28b.d(exc8) (described in ref. 16), 13LexAop-DmelGr28b.d (ref. 16), 13LexAop-DmojGr28b.d (this study), VT017654-Gal4.DBD (BDSC: 73303), 20E07-Gal4.AD (BDSC: 70586), UAS-CD8:GFP (BDSC: 32186), UAS-TdTomato (BDSC: 32221), UAS-Kir2.1 (BDSC: 6595) and UAS-CsChrimson (BDSC: 55136), obtained from the Bloomington *Drosophila* Stock Center (BDSC). *D. melanogaster* Egypt strain (EG16) was obtained from J. Pool and was reported in ref. 36. *D. mojavensis mojavensis* (NDSSC stock: 15081-1352.47), *D. mojavensis wrigleyi* (NDSSC stock: 15081-1352.29), *D. persimilis* (NDSSC stock: 14011-0111.51), *D. persimilis* (NDSSC stock: 14011-0111.24) and *D. mettleri* (NDSSC stock: 15081-1502.13) were obtained from the National *Drosophila* Species Stock Center (NDSSC). All *D. mojavensis* mutants and transgenics were generated as part of this study and maintained as homozygotes for the mutation or transgenic construct.

Temperature preference assays

Two-choice assays for temperature preference were carried out with groups of 3–5-day-old male flies raised under 12:12 h light/dark cycles^{10,22}. Flies were anaesthetized on ice, and groups of 15 flies were introduced to an array of individually addressable Peltier tiles (1-in squares) covered by a thin piece of black masking tape (Thorlabs). Flies were enclosed over the intersection of 4 Peltier tiles by a circular arena laser-cut out of a black acrylic sheet (1.8-in diameter) and covered by a sheet of glass coated with Sigmacote (Sigma Aldrich catalogue number SL2) to prevent flies from climbing on the walls and ceiling. Flies were given a choice between a base temperature (BT, 25 °C for all trials) and a test temperature (TT) in opposing quadrants for 3 min, and the spatial configuration of BT and TT quadrants was then reversed for an additional 3 min. Every change in configuration was interleaved by a brief 30-s step at 33 °C for *D. melanogaster*, *D. persimilis* and *D. mettleri* and 39 °C for *D. mojavensis* to ensure redistribution of the flies. Temperature setpoints were calibrated using an infrared thermal imaging camera (FLIR Systems). To record temperature preference behaviour, arenas were illuminated by infrared light, and videos of flies were recorded during each 3-min trial from above using a Chameleon3 USB camera (FLIR Systems). The position of each fly in every frame (375 frames s⁻¹) was determined and quantified using a preference index (PI), calculated as the difference between the number of flies in the BT quadrants and the number of flies in the TT quadrants, divided by the total number of flies (PI = (no. BT – no. TT)/total no.). For each TT condition, the PI values from the two trials (one at an initial configuration, and a second alternating the BT and TT quadrants) were averaged. A positive PI value indicates avoidance of the TT, whereas a negative value indicates attraction for the TT. A value of zero indicates no preference (equal time spent in both TT and BT). Two-tailed *t*-tests (threshold *P* = 0.05) were used to determine whether PI values were significantly different from zero. PI data are plotted using the notBoxPlot function (<https://github.com/raacampbell/notBoxPlot>).

Optogenetic preference assays

Two-choice assays for red-light preference in *D. melanogaster* flies expressing the redshifted channelrhodopsin CsChrimson were carried out with groups of 3–5-day-old male flies raised on standard fly food supplemented with 300 µM all-trans-retinal (Sigma Aldrich catalogue number R2500) in constant darkness and at room temperature (about 23 °C). Modelled after the two-choice assays for temperature preference described above, a behavioural arena was built to analyse fly behaviour when given a choice between blue light and red light (Extended Data Fig. 5f). A 16-by-16 array of light-emitting diodes (BTF-LIGHTING

WS2812B) controlled by a Raspberry Pi computer with the Adafruit CircuitPython NeoPixel module (https://github.com/adafruit/Adafruit_CircuitPython_NeoPixel) was placed underneath a laser-cut circular black acrylic arena (1.8-in diameter) separated by a diffuser (40% light transmission acrylic sheet). The arena was covered by a sheet of glass coated with Sigmacote to prevent flies from climbing on the walls and ceiling. Flies were anaesthetized on ice in groups of 25 individuals, and after a 6-min acclimation period (3 min in the dark followed by 3 min in all blue light), were given a choice between blue light and red light of equal brightness in opposing quadrants for 3 min, and then the spatial configuration of the quadrants was reversed for another 3 min. Flies were recorded from above using a camera (Arducam Raspberry Pi Camera OV5647), and the position of each fly was determined and quantified using a PI the same as described above for temperature preference assays. A positive PI value indicates avoidance of the red light, whereas a negative value indicates attraction to the red light. A value of zero indicates no preference (equal time spent in both blue- and red-light quadrants). Two-tailed *t*-tests (threshold *P* = 0.05) were used to determine whether PI values were significantly different from zero. For all behavioural experiments, sample sizes were not predetermined but were kept consistent across experiment type; approximate sample size was determined based on variance assessed by preliminary experiments. Collection of groups of flies was randomized and controlled for sex, species, time of day and strain.

Phylogenetic analysis

The phylogenetic tree representing *Drosophila* species relationships was adapted from <https://doi.org/10.6084/m9.figshare.5450602.v1>. A multiple sequence alignment of Gr28b.d proteins was generated using Clustal Omega (v1.2.3), and structural models of Gr28b.d were generated using AlphaFold3 (ref. 37).

Generation of reagents for transgenic flies

*DmojGr28b.d*¹¹ was generated using CRISPR–Cas9 technology³⁸. A target in exon D was found using the CRISPR Optimal Target Finder tool³⁹, and an RNA oligonucleotide was synthesized as single-guide RNA (sgRNA) using the MEGAscript T7 Transcription Kit (Invitrogen) with a DNA oligonucleotide containing the CRISPR target and the T7 promoter as a template. The sgRNA was cleaned using the MEGAClear Transcription Clean-Up Kit (Invitrogen). To create *D. melanogaster* flies bearing 13LexAop-*DmojGr28b.d*, the sequence of *DmojGr28b.d* CDS was predicted from the *DmojGr28b* genomic locus and amplified by PCR using an adult body *D. mojavensis* cDNA library (iScript Select cDNA Synthesis Kit, BioRad) as template and primers *DmojGr28b.d* F (5'-caaacATGTGGCCAATTGGAGGC AAC-3', modified Kozak sequence is in lowercase) and *DmojGr28b.d* R (5'-AATTCAATAATTAAATTAAATAAAAGAAT-3'). The PCR fragment was cloned into pCR8/GW/TOPO TA (Invitrogen) and sequenced. *DmojGr28b.d* cDNA was transferred into a p13xLexAop destination vector (described in ref. 16, by LR recombination, Invitrogen). The construct was then injected into *D. melanogaster* by BestGene. The *DmojGr28b.d* promoter > *DmelGr28b.d* CDS fusion was created using NEBuilder HiFi DNA Assembly (New England Biolabs). A fragment containing a region 1,500 base pairs upstream exon D from the *Gr28b* locus was amplified from *D. mojavensis* genomic DNA using primers *DmojGr28b.d* pF (5'-ACCTGGCACTGCATTTC-3') and *DmojGr28b.d* pR (5'-TATAGAGCGACTGCAACTTAGTTGC-3'). The fragment was then joined to *DmelGr28b.d* cDNA and the piggyBac vector pIM148-hr5-ie1p-mCherry (a gift from J. Parker) with NEBuilder HiFi DNA Assembly (New England Biolabs). To generate *DmojGr28b.d* promoter > CD8–GFP, the same promoter fragment was inserted upstream to the CD8–GFP fusion using NEBuilder HiFi DNA Assembly (New England Biolabs). The promoter fusions were sequenced, and the vector was purified using the NucleoBond Xtra Midi Plus EF kit (Macherey-Nagel).

Cell transfections

To study *Gr28b.d* from different species in cultured cells, *Gr28b.d*-coding sequences from *D. melanogaster*, *D. mojavensis*, *D. persimilis* and *D. mettleri* were cloned into standard expression vectors²⁰. The *Gr28b.d* was predicted from the *Gr28b.d* locus, and the CDS was amplified from a *D. persimilis* cDNA library that was generated using the iScript Select cDNA Synthesis Kit (BioRad) followed by a PCR reaction with the following primers: *DperGr28b.d* F (5'-caaaacATGAGTGGATTGGC-3', modified Kozak sequence is lowercase) and *DperGr28b.d* R (5'-CTAATT TGTATGATTGTTATTTATTG-3'). The PCR fragments were cloned into pCR8/GW/TOPO TA (Invitrogen) and sequenced (GenBank OQ624956). *DmojGr28b.d*, *DmelGr28b.d* and *D. mettleri Gr28b.d* (*DmetGr28b.d*) were amplified from respective cDNA libraries using the same methods with the following primers: *DmojGr28b.d* F (see above) and *DmojGr28b.d* R (see above), *DmelGr28b.d* F (5'-caaaacATGTCATTTACTTTGCG-3') and *DmelGr28b.d* R (5'-AAACGATTAATAATTATTCCAATC-3'), *DmetGr28b.d* F (5'-caaaacATGTGGCCAATTGGAGGCAACTGCTCAG-3') and *DmetGr28b.d* R (5'-CTAACCGTATGATTCGATATATTATGAAAC GCCTCACACAGTC-3') (modified Kozak sequences are in lowercase). For expression in mammalian cell culture, *DmelGr28b.d*, *DmojGr28b.d*, *DperGr28b.d* and *DmetGr28b.d* cDNA in pCR8/GW/TOPO TA (Invitrogen) sequences were transferred into pcDNA3.1/nV5-DEST by LR reaction (ThermoFisher). HEK293T (ATCC) cells were cultured in Dulbecco's modified Eagle medium (ThermoFisher) supplemented with 10% FBS and 1% penicillin–streptomycin (100 U ml⁻¹ and 100 µg ml⁻¹, respectively; from Fisher). Cell cultures were maintained in 25 cm² tissue culture flasks with plug seal caps at 37 °C with 5% CO₂. For electrophysiological recordings, cells were grown on coverslips and co-transfected with 0.5 µg of pcDNA3.1-GFP vector and 1.5 µg of either one of the vectors harbouring *DperGr28b.d*, *DmelGr28b.d*, *DmojGr28b.d* or *DmetGr28b.d*, and mixed with 4 µl of transfection reagent and 200 µl of transfection buffer (jetPRIME in vitro DNA & siRNA transfection reagent, PolyPlus). After transfection, cells were incubated for 24–48 h at 37 °C with 5% CO₂ to allow for gene expression. *Drosophila* S2R+ (Drosophila Genomics Research Center, DGRC Stock 150) were cultured in GlenClone Schneider's Insect Medium (Sigma Aldrich) supplemented with 10% FBS and 1% penicillin–streptomycin at room temperature. S2R+ cells were grown on coverslips and transfected with pAC-GW expression vectors harbouring *DmelGr28b.d* and co-transfected with pAC-GFP as described above. After transfection, the cells were incubated for 72–120 h at room temperature to allow for gene expression. All cell lines were authenticated by the manufacturer and tested for mycoplasma contamination.

Electrophysiology

Whole-cell patch-clamp electrophysiology experiments were performed on HEK293T and S2R+ transfected cells identified by GFP fluorescence. The intracellular solution for recordings with HEK293T cells contained 140 mM K-gluconate, 1 mM MgCl₂, 1 mM EGTA, 10 mM HEPES; pH was adjusted to 7.2 ± 3 and the osmolarity was adjusted to 283 ± 5 mOsm with sucrose. The intracellular solution for recordings with S2R+ cells contained 140 mM K-gluconate, 2 mM MgCl₂, 0.01 mM CaCl₂, 1 mM EGTA, 5 mM HEPES and 1 mM Na₂ATP; pH was also adjusted to 7.2 ± 3, and the osmolarity was adjusted to 290 ± 5 mOsm with sucrose. All internal solutions were stored at -20 °C. The extracellular solution for recordings with all cells contained 140 mM NaCl, 5 mM KCl, 1 mM CaCl₂, 1 mM HEPES and 10 mM glucose; pH was adjusted to about 7.2 with NaOH, and the osmolarity was adjusted to 305 ± 5 mOsm with sucrose. The resistance of patch pipettes ranged from 3 to 7 MΩ. Recordings were obtained with an AxoPatch 200B amplifier (Axon Instruments), analysed with Axograph software, scaled to 1× output gain, lowpass-filtered with 5 kHz, and digitized with a Digidata 1320A (Axon Instruments). Bath offset and capacitance were compensated; series resistance was 9.5 ± 5.5 MΩ without compensation. Recordings

were made at about 19–23 °C, and heating was achieved by using an inline heater (HPT-2A, ALA Scientific Instruments), TC-20 temperature controller (NPI Electronics) and a T-384 thermocouple (Physitemp Instruments) tethered to the electrode holder, such that the tip of the thermocouple was at a close distance to the electrode. Cells were held at constant -60 mV, and currents were monitored during heat stimulation. To obtain current–voltage relationships, voltage ramps from -100 to 100 mV were applied every 200 ms, such that I/V curves were obtained before, during and after 40 s heat stimulations at 40 °C. Arrhenius plots were generated from recordings both in HEK293T and S2R+ cells in IgorPro (WaveMetrics). First, recordings (including current and temperature traces) from cells expressing *Gr28b.d* from *D. melanogaster*, *D. persimilis*, *D. mojavensis* and *D. mettleri* were filtered using a cutoff frequency of 200 Hz on Axograph software. Next, currents were normalized to the maximum value for each recording, log-transformed and plotted as a function of the reciprocal of temperature in kelvin. The temperature threshold of activation was calculated from the intersection point of the two lines, generated by linear fits to the shallowest and steepest regions of the plots. *Q*₁₀ values were calculated using the following equation: $Q_{10} = (I_2/I_1)^{(10/T_2 - 1/T_1)}$. *I*₁ was the value of the current taken at the lower temperature T₁, whereas the *I*₂ value was taken at the higher temperature T₂, before and after the temperature threshold. Temperature threshold distributions and *Q*₁₀ values are displayed using the notBoxPlot function (see above) in MATLAB, in which means are shown as thick lines and the boxes represent standard deviation from the mean (shaded boxes) and 95% confidence interval (unshaded boxes).

D. mojavensis embryo microinjection

Microinjections of *D. mojavensis* embryos were carried out using a Leica DM IRB microscope equipped with a Narishige IM 300 Microinjector and MN-153 micromanipulator, and pulled glass capillaries (1B100-F4, 1.00 mm OD/0.58 ID) with a Sutter P-97 micropipette puller. Before injections, *D. mojavensis* flies were reared in cages with *Opuntia* cactus juice agar plates to promote egg laying, and eggs were collected in 45–60-min intervals, aligned on coverslips, and staged according to the developmental time point. The eggs were left to dry for 1–3 min to allow adhesion to the coverslip and were then covered with olive oil to prevent further drying during the injection process. For CRISPR injections, the sgRNA oligonucleotide was mixed with EnGen Spy Cas9 NLS (New England Biolabs) and injected into *D. mojavensis* embryos at a final concentration of 187.5 ng µl⁻¹ sgRNA and 300 ng µl⁻¹ Cas9 protein. The presence of the mutation was confirmed by sequencing of the genomic region containing the CRISPR target. For piggyBac injections, plasmid vectors bearing transgenic constructs were mixed with mRNA for the hyperactive pBase (made from a linearized vector containing the hyperactive transposase as template with HiScribe T7 ARCA mRNA Kit, New England Biolabs) and purified with RNAClean SPRI XP beads (Beckman Coulter) at a final concentration of 300 ng µl⁻¹ of DNA and mRNA. Injection mixtures were then transferred into pulled glass capillaries. The filled injection needles were loaded onto the microinjector, and stage-1–2 embryos were injected through the chorion from the posterior end. After injection, embryos were washed with 95% ethanol to remove the oil and soaked in deionized water for 10 min for rehydration. Coverslips with the embryos were then placed in softened cornmeal agar medium, and embryos were monitored to ensure viability. Transgenics were screened for fluorescence from the mCherry transformation marker (driven by the ie1 promoter as described in ref. 40) using a stereo microscope equipped with a fluorescence adaptor (NIGHTSEA Model SFA).

RNA sequencing and expression analyses

To extract RNA from *D. mojavensis* aristae, the tissue was homogenized in TRIzol (Invitrogen), and RNA was purified using the RNeasy Micro Kit (Qiagen). RNA sample quality evaluation, library preparations

Article

and sequencing were carried out at the NUSeq Core Facility, Northwestern University. RNA integrity and concentration were assessed by on-chip electrophoresis with the Bioanalyzer (Agilent). The SMART-seq V4 Ultra low input RNA kit (Takara Bio) was used to construct a cDNA library from total RNA, and single-end sequencing was carried out with the Illumina HiSeq2000 sequencing system. Reads were trimmed to 75 bp and read quality was assessed with FastQC; none was flagged as poor quality out of the 19,107,080 total reads. The *D. mojavensis* genome was indexed, and the reads were aligned onto the genome using STAR with default parameters, as well as in Geneious Prime (Dotmatics) for visualization with 92.12% of reads uniquely mapped to the genome. Read counts per gene were obtained from the alignment through STAR, and RPKM values were calculated in R for each gene using the gene lengths and total mapped reads. The heat map for visualizing relative expression of key genes with $\log_2[\text{RPKM} + 1]$ was generated in R using the image function.

Immunostaining of *Drosophila* brains

D. melanogaster and *D. mojavensis* brains were dissected from 3–5-day-old adults in phosphate-buffered saline (PBS) and stained with antibodies using standard protocols. Following dissections, brains were fixed with 4% paraformaldehyde for 30 min, washed three times with PBS + 0.2% Triton X-100 (PBST), and incubated with PBST + 3% bovine serum albumin (BSA) for 1 h. Following rinsing and blocking, tissues were incubated with primary antibody diluted in PBST + 3% BSA (1:1,000 anti-GFP and 1:20 nc82) for about 16 h, and after rinsing six times with PBST, were then incubated with secondary antibody diluted in PBST + 3% BSA (1:2,000 AlexaFluor 488 and 1:250 AlexaFluor 594) for about 16 h. To prepare for imaging, brains were washed six times with PBST and mounted in VECTASHIELD (Vector Laboratories). The primary antibodies used were mouse anti-nc82 (DSHB) and chicken anti-GFP (ab13970, Abcam), and the secondary antibodies used were AlexaFluor 488 donkey anti-chicken IgY and AlexaFluor 594 donkey anti-mouse IgY (Jackson ImmunoResearch Laboratories).

Fluorescence microscopy

Confocal imaging of *D. melanogaster* and *D. mojavensis* antennae and brains was performed on a Zeiss LSM 510 confocal microscope equipped with argon 450–530 nm, helium–neon 543 nm and helium–neon 633 nm lasers and a Zeiss LCI Plan-Neofluar/0.8 DIC Imm Corr ×25 objective at a resolution of 1,024 × 1,024 pixels. Maximum projections were obtained from stacks taken at 1 μm steps. For antennae, autofluorescence of the cuticle was excited with a 561-nm laser, and emitted light was captured with a 575-nm longpass filter. Images were processed in Fiji (ImageJ).

Labelling of projection neurons by electroporation

Labelling of *Drosophila* TPNs by electroporation was performed according to previously described methods with some modifications^{41–43}. Adult flies were anaesthetized by brief cold exposure in an ice bath and brains were dissected in artificial haemolymph (AHL; pH 7.3) containing 103 mM NaCl, 3 mM KCl, 26 mM NaHCO₃, 1 mM NaH₂PO₄, 8 mM trehalose dihydrate, 10 mM dextrose, 5 mM TES, 4 mM MgCl₂ and 1.5 mM CaCl₂ (adjusted to 270–275 mOsm and equilibrated with 95% O₂ and 5% CO₂). Brains were pinned to a SYLGARD-lined dish (Dow Corning 184 Silicone Elastomer, Fisher catalogue number NC9285739) and perfused with AHL (flow rate of 1–2 ml min⁻¹) at 25 °C using an in-line heater–cooler (Warner, catalogue number SC-20) controlled by a dual-channel bipolar temperature controller (Warner Instruments, CI-200A). Glass electrodes (1B150F-5) were prepared using a Sutter P-97 puller to an open tip resistance of 2–5 MΩ and back-filled with 1–2 μl of 100 mg ml⁻¹ AlexaFluor 488 3 kDa, AlexaFluor 488 10 kDa or AlexaFluor 594 10-kDa dextran dye (ThermoFisher catalogue numbers D34682, D22910 and D22913, respectively). Dye-filled pipettes were loaded onto a micropipette holder (WPI, MPH6S) controlled by a Sutter QUAD

micromanipulator, and a silver wire was used to generate d.c. voltage pulses with one terminal inserted into the glass pipette and the other terminal placed in the bath solution adjacent to the brain.

As a guide, the electrode tip was targeted to the axon terminals of hot cells (HCs) within the PAL using expression of CD8–GFP in *D. mojavensis* under the control of the *DmojGr28b.d* promoter, or expression of UAS-CD8–GFP or UAS-TdTomato in *D. melanogaster* under control of HC-Gal4. To label TPNs in *D. persimilis* and *D. mettleri*, axon terminals of HCs were visualized by implementing an arista dye staining procedure, and to label olfactory projection neurons in *D. mojavensis*, olfactory glomeruli were visualized with an antennal dye staining procedure. Adult flies were anaesthetized by brief cold exposure and mounted on a custom-made head-restraint apparatus, and both aristae were cut with forceps. The arista nerve was loaded using a pipette filled with 50 mg ml⁻¹ TexasRed dextran dye solution (3 kDa, ThermoFisher catalogue number D3329), and flies were subsequently incubated at room temperature for 1–3 h. For labelling of olfactory glomeruli, the same procedure was performed as above but the aristae were not cut, and the dye was placed directly on the third antennal segment. Brains were then dissected in AHL and prepared for electroporation as described above.

Electroporation of the dye was performed using an S48 stimulator (Grass) to deliver a 50-V pulse with a duration of 10 ms and a frequency of 0.2 Hz (5-s inter-stimulus interval) for 3–10 min. To reduce background fluorescence of excess extracellular dye and allow for transport of the internalized dextran-conjugated dye, brains were perfused in AHL for at least 15–20 min after electroporation. Dye fills were monitored with an upright Zeiss Examiner.Z1 microscope with a Zeiss W Plan-Apochromat ×40, 0.9 numerical aperture water-immersion objective. Brains were imaged at 945 nm by a Chameleon Ultra Ti:sapphire laser (Coherent) and detected using a photomultiplier tube through a bandpass filter (490–560 nm for AlexaFluor 488 and GFP, or 580–630 nm for AlexaFluor 594 and TdTomato) using a modified Ultima 2-photon laser scanning microscope (Bruker). Two different mounting orientations were used, the ‘front view’ and ‘top view’. For the front view, brains were laid flat and pinned on a SYLGARD-lined dish and were scanned on the anterior-posterior axis of the brain. For the top view, brains were rotated 90° and pinned in a custom SYLGARD-lined dish such that the dorsal surface of the brain was facing upwards (towards the objective) and were scanned on the dorsal–ventral axis of the brain (Extended Data Fig. 3a). Images were acquired at a resolution of 1,024 × 1,024 pixels using PrairieView software v5.2 (Bruker) and processed as described below.

Neuron reconstructions

D. melanogaster brain volume images, neuron skeletons and brain regions of interest were downloaded from the Hemibrain:v1.2.1 dataset⁴⁴ using Python scripts and displayed in ParaView (v5.11.0). Three-dimensional reconstructions of TPNs filled by electroporation of dextran dyes were generated from two-photon microscopy z-stacks. z-stacks were processed in Fiji (ImageJ) to optimize contrast, and LH and calyx volumes were segmented along all z-slices using the Segmentation Editor (built-in Fiji plugin) and were then used as a reference channel for within-species image registration as well as for visualization alongside 3D neuron reconstructions (Extended Data Fig. 3b). To align images to reference neuropils for each species, we used the Computational Morphology Toolkit (<http://www.nitrc.org/projects/cmtk>) software as well as the Registration GUI plugin for Fiji (ImageJ; <https://github.com/jefferis/fiji-cmtk-gui>). Once each z-stack was registered, we then used neuTube⁴⁵ to trace the neuronal projection in each image, first by thresholding the images to create a binary mask, and second by using the mask as input to neuTube for automatic tracing in three dimensions. For most z-stacks, favourable signal to noise allowed us to directly threshold the images; however, for some fills that had higher background or off-target labelling, we used the Simple Neurite Tracer program⁴⁶ to manually trace the branches and produce a binary mask as input for neuTube automatic tracing (see Extended Data Fig. 3c for

representative reconstructions of *D. melanogaster* and *D. mojavensis* TPN-V alongside two-photon z-stack maximum projections). With 3D reconstructions of neuron skeletons and brain volumes in hand, we then visualized them together in neuTube, and exported neuron skeletons as SWC files for further analysis (see below).

Quantification of projection neuron anatomy

To quantify branching patterns of reconstructed neurons, we used the CAJAL package³⁰. For each species (*D. melanogaster*, *D. mojavensis*, *D. persimilis* and *D. mettleri*), we used 3D reconstructions of TPN-V cropped in the LH and calyx separately as input ($n = 5$ reconstructions per species). First, the software samples a set of points (100) along each neuron skeleton and generates a pairwise Euclidean distance matrix. Second, it performs optimal matching of each cell Euclidean matrix with each other by computing the Gromov–Wasserstein distance, quantifying the amount of deformation needed to convert one neuron skeleton to another. This Gromov–Wasserstein pairwise distance matrix can be thought of as the distances between each neuron reconstruction in intrinsic cell morphology space (Extended Data Fig. 3d). As the CAJAL analysis is agnostic to spatial differences in innervation of brain regions, we separately quantified the centre of mass (COM) of each LH and calyx projection pattern (Extended Data Fig. 3e). For each z-stack, we produced a maximum-intensity projection centred on the LH or calyx neuropil (that is, cropped by a square at the edge of the neuropil outline; defined using the 3D volume as defined above); we then transformed these images to normalize dimensions and measured the COM of the 2D projection using the COM function in Fiji (ImageJ). We also repeated this analysis on the basis of an ‘artificial’ projection of a *D. melanogaster* EM volume reconstruction. With COM measurements for each cell, we calculated pairwise taxicab distances. Finally, we took the Gromov–Wasserstein pairwise distance matrix (from CAJAL) and the pairwise taxicab distance matrix (from COM), normalized them both to their respective maximum values, and we then summed these two measures to produce a matrix of cell–cell distances. Distances were used for hierarchical clustering (Extended Data Fig. 3f) using the Agglomerative Clustering function from the scikit-learn Python module (<https://github.com/scikit-learn/scikit-learn>, using Gower distance as a similarity measure) and visualized using the ‘dendrogram’ function in the SciPy Clustering package. Distances were also independently used for UMAP embedding (from the umap-learn package). We used SigClust⁴⁷ to test for statistically significant clustering ($P = 0.05$).

Connectomics

Identification of postsynaptic targets and quantification of synaptic weights of hot TRNs in the *D. melanogaster* connectome was carried out by querying the EM Hemibrain:v1.2.1 (ref. 44; neuroimage.janelia.org/; Fig. 4f). Using the Common connectivity function, the common outputs of the three hot TRNs were identified and ranked (threshold >9 synapses). Note that the top common synaptic output of hot TRNs is TPN-V, followed by TPN-Ia and TPN-Ib. TPN-V stands as the overall top common synaptic output of the hot TRNs (receiving 14% of all output synapses), as well as if one excludes connections to local interneurons (cells that do not leave the PAL), in which case TPN-V receives 26% of all hot TRN output synapses (564/2146 synapses; Fig. 4f). Reconstruction of the pathways from hot TRNs of the arista to TLHON-II (Extended Data Fig. 5a) was performed using the Shortest path function, by identifying direct hot-specific TPN connections from each hot TRN to TLHON-II (neuron ID 514068564). We then summed all synaptic connections from TRNs and other hot-specific TPNs to calculate the percentage of synapses that connect to TPN-V, and the percentage of total synapses from TPN-V to TLHON-II, respectively. Identification of the synaptic loci between TPN-V and TLHON-I and TLHON-II (Extended Data Fig. 5c) was carried out using the Synapses for connection function, restricting output to the right-side LH for each respective connection: TPN-V to TLHON-I (ref. 28), and TPN-V to TLHON-II, respectively. Synaptic loci coordinates

were then imported into ParaView (v5.11.0) and overlaid on the skeleton for TPN-V.

Reporting summary

Further information on research design is available in the Nature Portfolio Reporting Summary linked to this article.

Data availability

All data are available in the main paper and Extended Data Figs. 1–7. Maps were created in MATLAB and traced in Adobe Illustrator; all other illustrations were created in Adobe Illustrator. Gr28b.d-coding sequences from *D. persimilis* (GenBank OQ624956), *D. mojavensis* (GenBank OQ621410) and *D. mettleri* (GenBank PP885916) are available via GenBank. Raw read sequences from RNA-seq of samples from *D. mojavensis* aristae are available via the Sequence Read Archive of the National Center for Biotechnology Information with the BioProject ID PRJNA948454. The following database was also used: EM Hemibrain:v1.2.1 (<https://neuroimage.janelia.org/>). Source data are provided with this paper.

Code availability

No custom algorithms or computer code was produced as part of this work.

36. Sprengelmeyer, Q. D. et al. Recurrent collection of *Drosophila melanogaster* from wild African environments and genomic insights into species history. *Mol. Biol. Evol.* **37**, 627–638 (2020).
37. Abramson, J. et al. Accurate structure prediction of biomolecular interactions with AlphaFold 3. *Nature* **630**, 493–500 (2024).
38. Doudna, J. A. & Charpentier, E. Genome editing. The new frontier of genome engineering with CRISPR-Cas9. *Science* **346**, 1258096 (2014).
39. Gratz, S. J. et al. Highly specific and efficient CRISPR/Cas9-catalyzed homology-directed repair in *Drosophila*. *Genetics* **196**, 961–971 (2014).
40. Masumoto, M., Ohde, T., Shioiri, K., Yaginuma, T. & Niimi, T. A baculovirus immediate-early gene, ie1, promoter drives efficient expression of a transgene in both *Drosophila melanogaster* and *Bombyx mori*. *PLoS ONE* **7**, e49323 (2012).
41. Caron, S. J., Ruta, V., Abbott, L. F. & Axel, R. Random convergence of olfactory inputs in the *Drosophila* mushroom body. *Nature* **497**, 113–117 (2013).
42. Hayashi, T. T. et al. Mushroom body input connections form independently of sensory activity in *Drosophila melanogaster*. *Curr. Biol.* **32**, 4000–4012.e5 (2022).
43. Li, J., Mahoney, B. D., Jacob, M. S. & Caron, S. J. C. Visual input into the *Drosophila melanogaster* mushroom body. *Cell Rep.* **32**, 108138 (2020).
44. Scheffer, L. K. et al. A connectome and analysis of the adult *Drosophila* central brain. *eLife* <https://doi.org/10.7554/eLife.57443> (2020).
45. Feng, L., Zhao, T. & Kim, J. neuTube 1.0: A new design for efficient neuron reconstruction software based on the SWC format. *eNeuro* <https://doi.org/10.1523/ENEURO.0049-14.2014> (2015).
46. Arshadi, C., Gunther, U., Eddison, M., Harrington, K. I. S. & Ferreira, T. A. SNT: a unifying toolbox for quantification of neuronal anatomy. *Nat. Methods* **18**, 374–377 (2021).
47. Huang, H., Liu, Y., Yuan, M. & Marron, J. S. Statistical significance of clustering using soft thresholding. *J. Comput. Graph. Stat.* **24**, 975–993 (2015).

Acknowledgements We thank M. Stensmyr, T. Bozza, H. Lee and members of the Gallio Lab for comments; D. Bennett, A. Park, P. Seng, I. Baker and especially A. Kuang, J. Hua and P. Laminette for technical assistance in the early stages of the work; R. Suhendra for help with data analysis; and M. Stensmyr for the gift of fly drawings in Figs. 1, 3 and 5. This work was supported by National Institutes of Health, National Institute of Neurological Disorders and Stroke grants R01NS086859, R21NS130554 (to M.G.) and 1F31NS129270 (to M.C.), the PEW Scholars Program (M.G.) and a grant from the Trienens Institute for Sustainability and Energy at Northwestern University (A.P.).

Author contributions Conceptualization: M.G., A.P. and M.C.; behavioural experiments and analysis: M.C., A.A., E.E.Z., I.D.M.-G. and J.M.S.; electrophysiology and analysis: O.M.A., M.C. and Y.S.; CRISPR mutants and transgenesis: M.C. and A.P.; RNA sequencing and analysis: E.E.Z., A.P. and M.C.; *in vivo* electroporation and analysis: M.C. and M.H.A.; microscopy: H.G., M.C. and M.H.A.; visualization: M.G. and M.C.; funding acquisition: M.G.; supervision: M.G. and A.P.; writing: M.G. and M.C.

Competing interests The authors declare no competing interests.

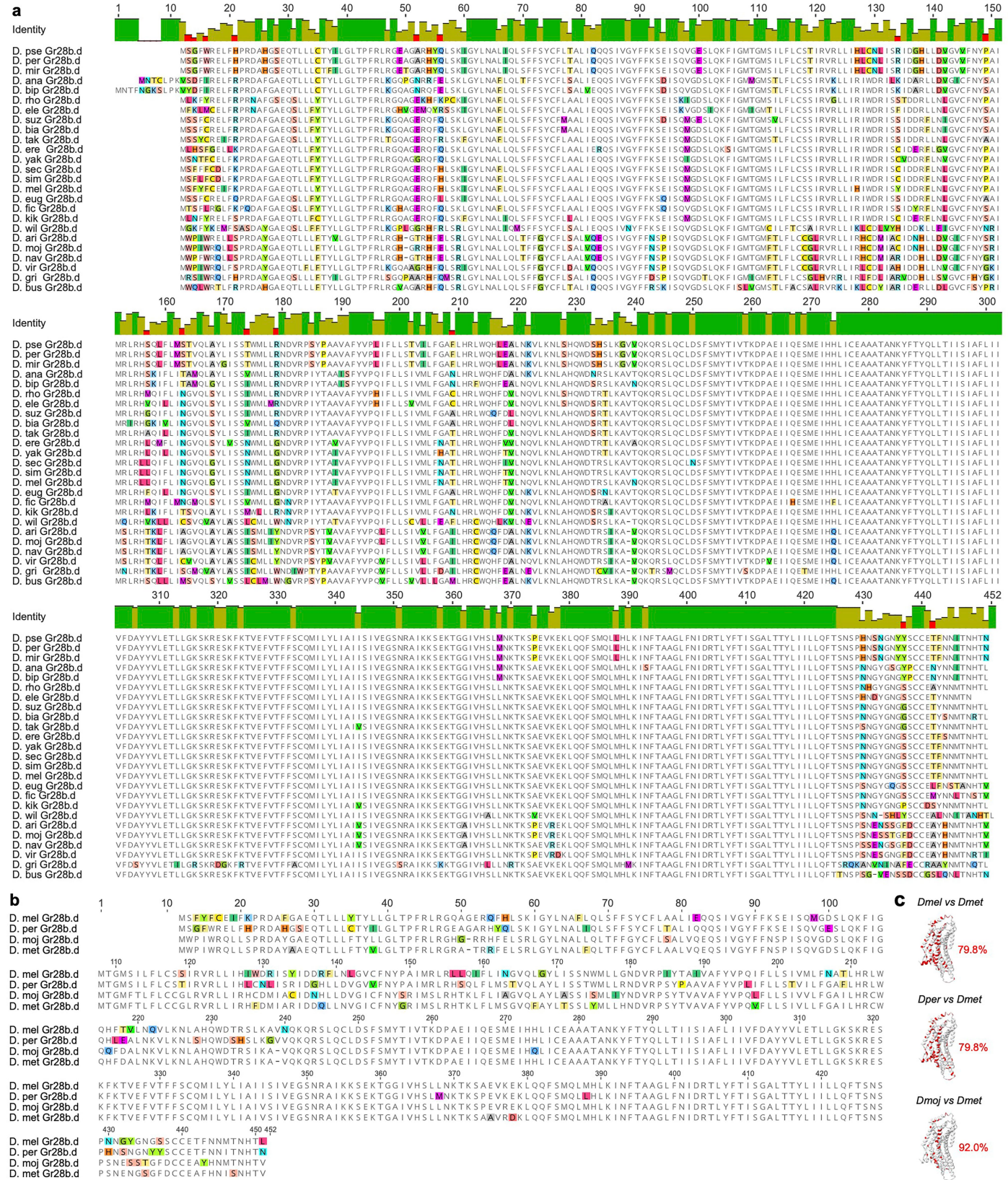
Additional information

Supplementary information The online version contains supplementary material available at <https://doi.org/10.1038/s41586-025-08682-z>.

Correspondence and requests for materials should be addressed to Alessia Para or Marco Gallio. **Peer review information** *Nature* thanks Sophie Caron and the other, anonymous, reviewer(s) for their contribution to the peer review of this work. Peer reviewer reports are available.

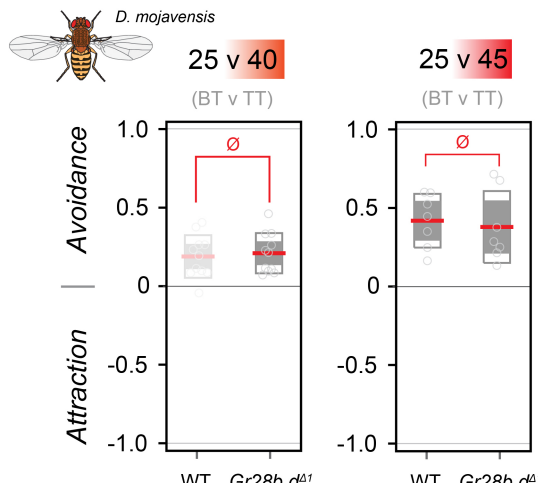
Reprints and permissions information is available at <http://www.nature.com/reprints>.

Article



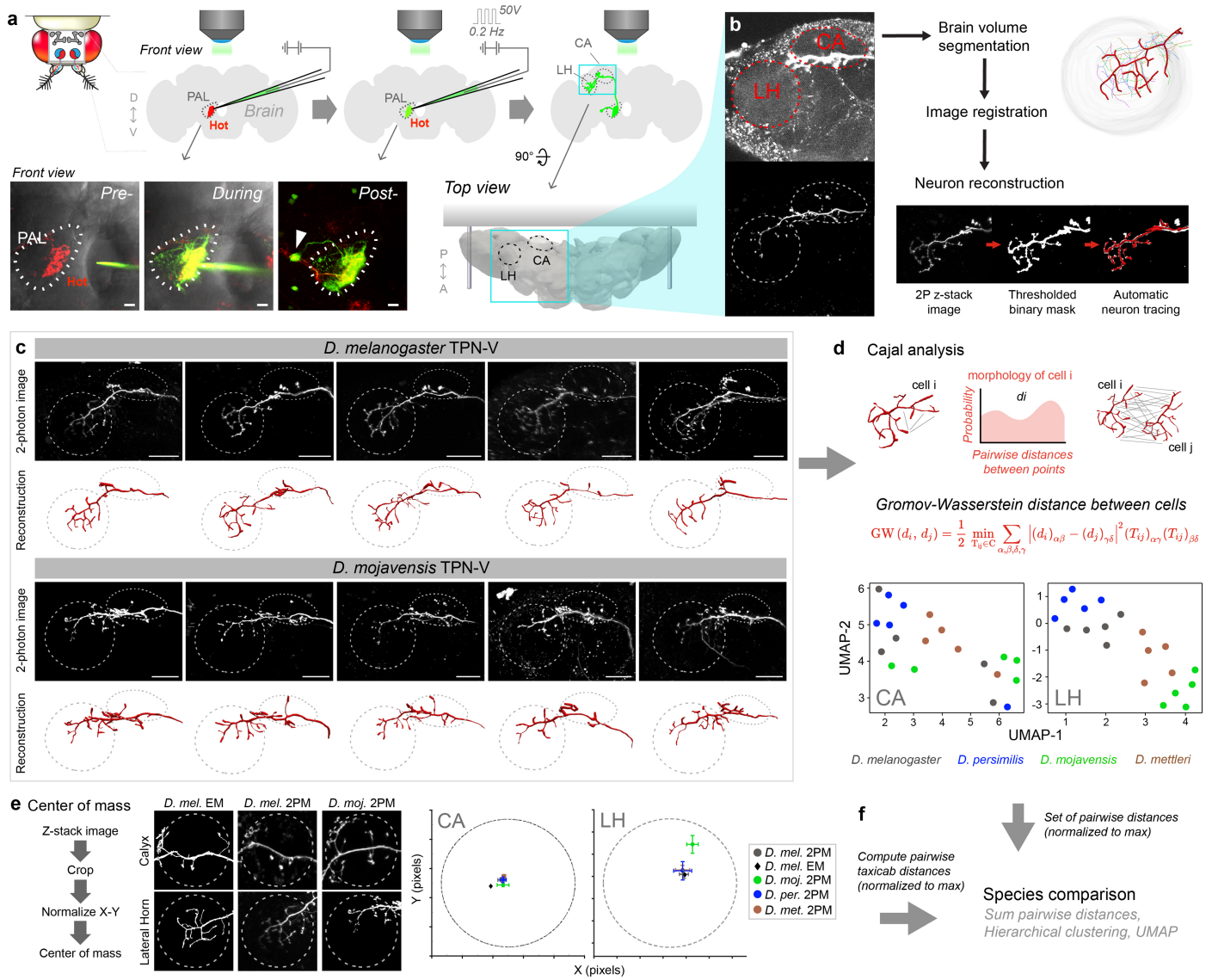
Extended Data Fig. 1 | Alignment of Gr28b.d protein sequences across Drosophila species. (a) Multiple alignment of Gr28b.d protein sequences from 25 *Drosophila* species (names abbreviated to first three letters, e.g. *D. mel* = *D. melanogaster*), (b) and of the 4 species *D. melanogaster*, *D. persimilis*, *D. mojavensis*, and *D. mettleri*. (c) Location of amino acid differences between

the indicated species (red=different). (histogram: bars = mean pairwise amino acid sequence identity across species, green = 100%, yellow = <100% and $\geq 30\%$, orange = <30%; highlighted residues below denote divergence from the consensus sequence and are colored by amino acid identity using the default Geneious color scheme).

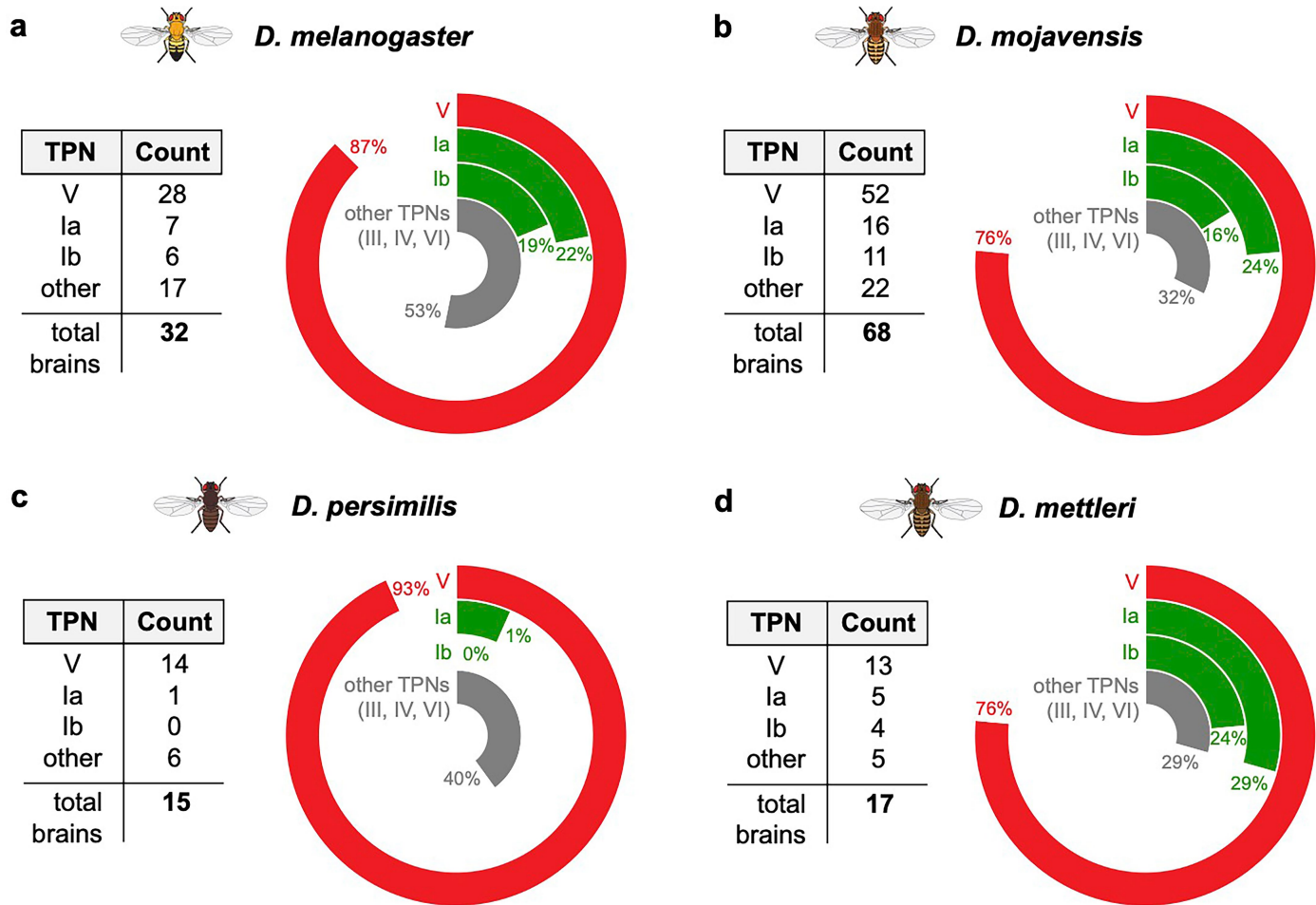


Extended Data Fig. 2 | The *D. mojavensis* *Gr28b.d* null mutant displays normal avoidance of noxious heat. For each panel, the data plotted on the left is the preference index for wild-type *D. mojavensis* (WT), and the data plotted on the right is the preference index of *D. mojavensis* *Gr28b.d*^{Δ¹} mutants. In all cases, flies were given a choice between 25 °C and a TT of 40° or 45 °C, respectively. The transparent box on the left represents wild type *D. mojavensis* data re-drawn from Fig. 1 to allow for direct comparison. Ø indicates the wild type and mutant preference distributions are not statistically different (two-tail two sample t-test, * $p < 0.05$; $p = [0.678, 0.720]$ for WT vs. mutant for 40 °C and 45 °C, respectively; red lines=mean, grey boxes=one standard deviation, empty boxes=95% confidence interval for the mean, empty circles=datapoints; each datapoint is one group of 15 flies; $N = 11$ datapoints/condition).

Article



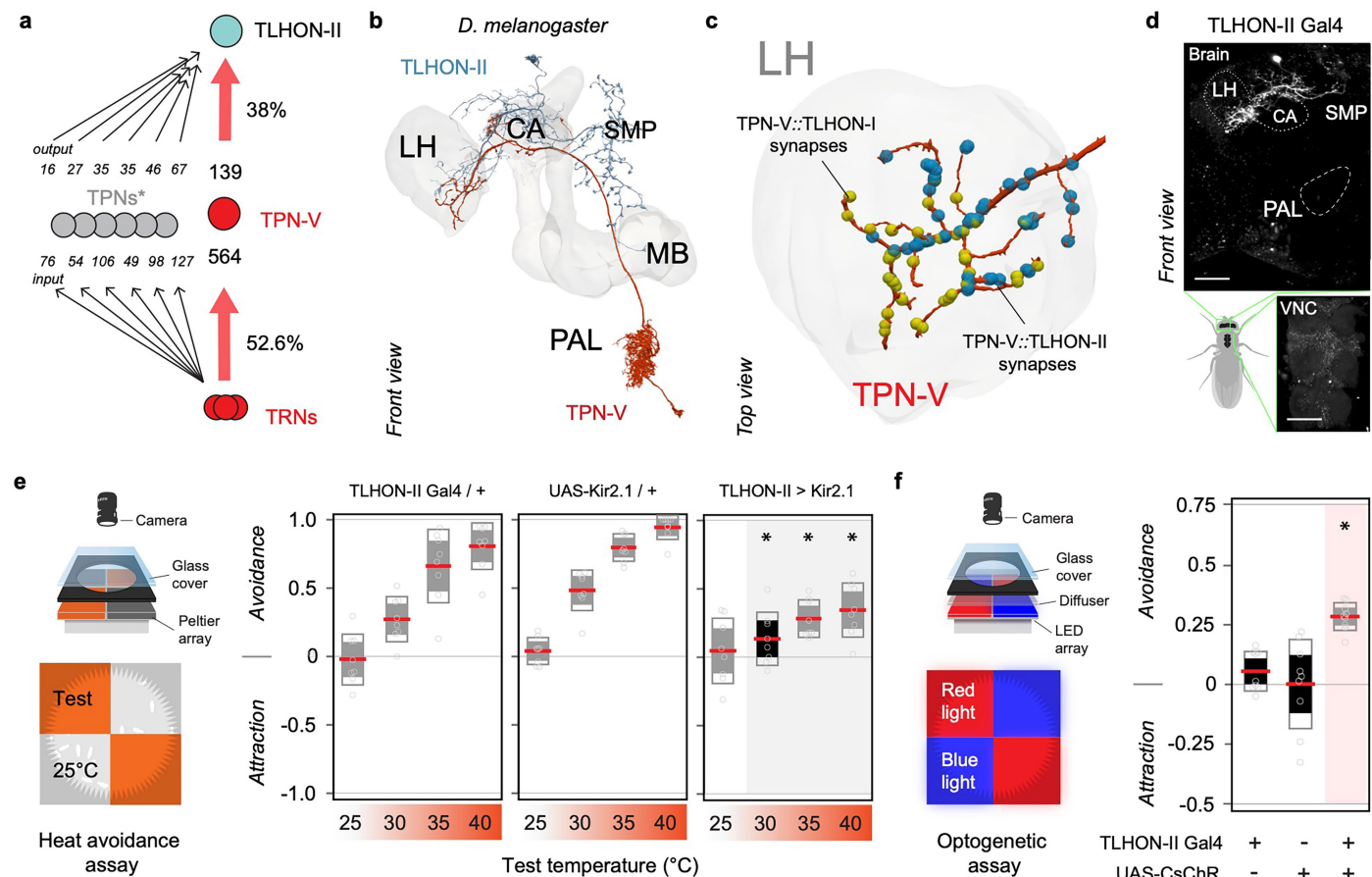
Extended Data Fig. 3 | Labelling, reconstructing, and analyzing thermosensory projection neurons in *Drosophila* brains. (a) TPN labeling strategy using electroporation of dextran-conjugated dyes, followed by imaging in Front view (on anteroposterior axis) and Top view (on dorsoventral axis) of the brain. (b) Following the acquisition of 2-photon z stacks, 2D outlines of brain regions are segmented to produce a 3D model of the CA and LH which is used for image registration (to align images to a representative brain for each species). Neurons are traced in the registered volumes using neuTube and visualized alongside the 3D CA and LH volumes. (c) Maximum projections and corresponding 3D neuronal reconstructions of five labelled TPN-V in *D. melanogaster* and *D. mojavensis* brains. (d) Neuron reconstructions are exported in SWC format, and intrinsic neuronal morphology is quantified with the CAJAL package. UMAP embedding of pairwise distances from CAJAL



Extended Data Fig. 4 | Frequency of Thermosensory Projection Neuron cell types labelled in dye electroporation experiments across *Drosophila* species. (a-d) Counts (tables) and frequencies (visualized as radial bar graphs) of Thermosensory Projection Neuron (TPN) cell types labeled in dye-filling experiments, arranged by species. Included are all experiments that successfully labelled a small number of TPNs (up to 3-4) allowing unambiguous identification

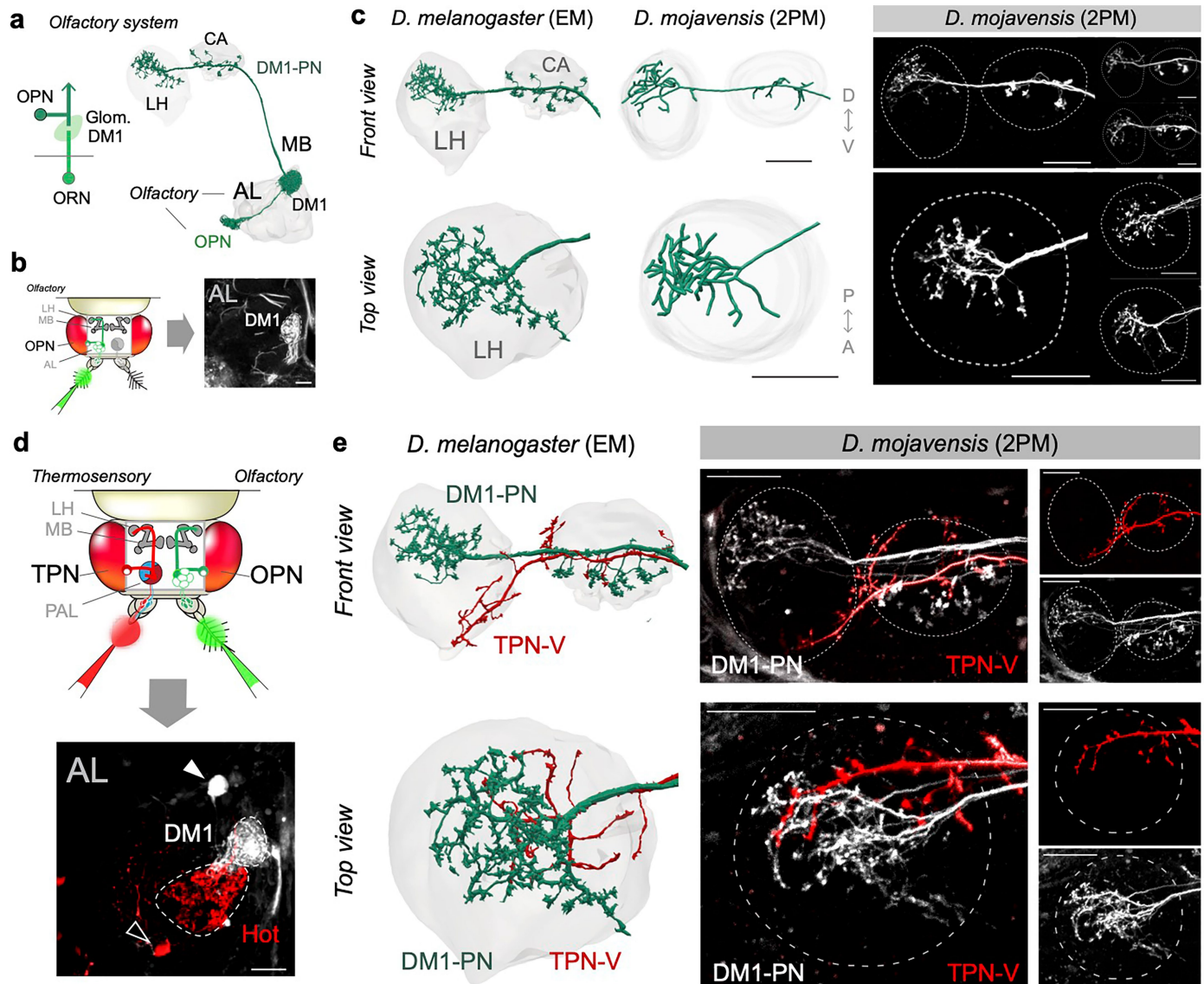
of each cell type. We excluded experiments in which only local interneurons of the PAL were labeled, where too many TPNs were labeled, or where labeling of olfactory projections prevented us from classifying TPNs. (Note that individual percents for cell types add up to more than 100% due to double- and triple-labeling of TPNs in the same brains).

Article



Extended Data Fig. 5 | Thermosensory Lateral Horn Output Neuron II (TLHON-II) is the primary output of TPN-V and is critical for heat avoidance behavior in *D. melanogaster*. (a) Connectomic diagram illustrating the pathways that relay temperature information from the hot thermosensory receptor neurons (TRNs) to the Thermosensory Lateral Horn Output Neuron II (TLHON-II). TPN-V is the major output of the aristal hot TRNs (comprising 52.67% of hot TRN output synapses to TPNs) and the major direct path of connectivity from hot TRNs to Thermosensory Lateral Horn Output Neuron II (TLHON-II), which is in turn the major target of TPN-V (black arrows represent alternative direct pathways of connectivity between hot TRNs and TLHON-II, Ns=number of synapses). (b) *D. melanogaster* EM reconstruction of TPN-V (red) and TLHON-II (light blue). (c) TPN-V::TLHON-I synapses (yellow dots) and TPN-V::TLHON-II synapses (blue dots) tile the TPN-V axonal arbor within the LH (synapse location was reconstructed from EM data, see methods for details).

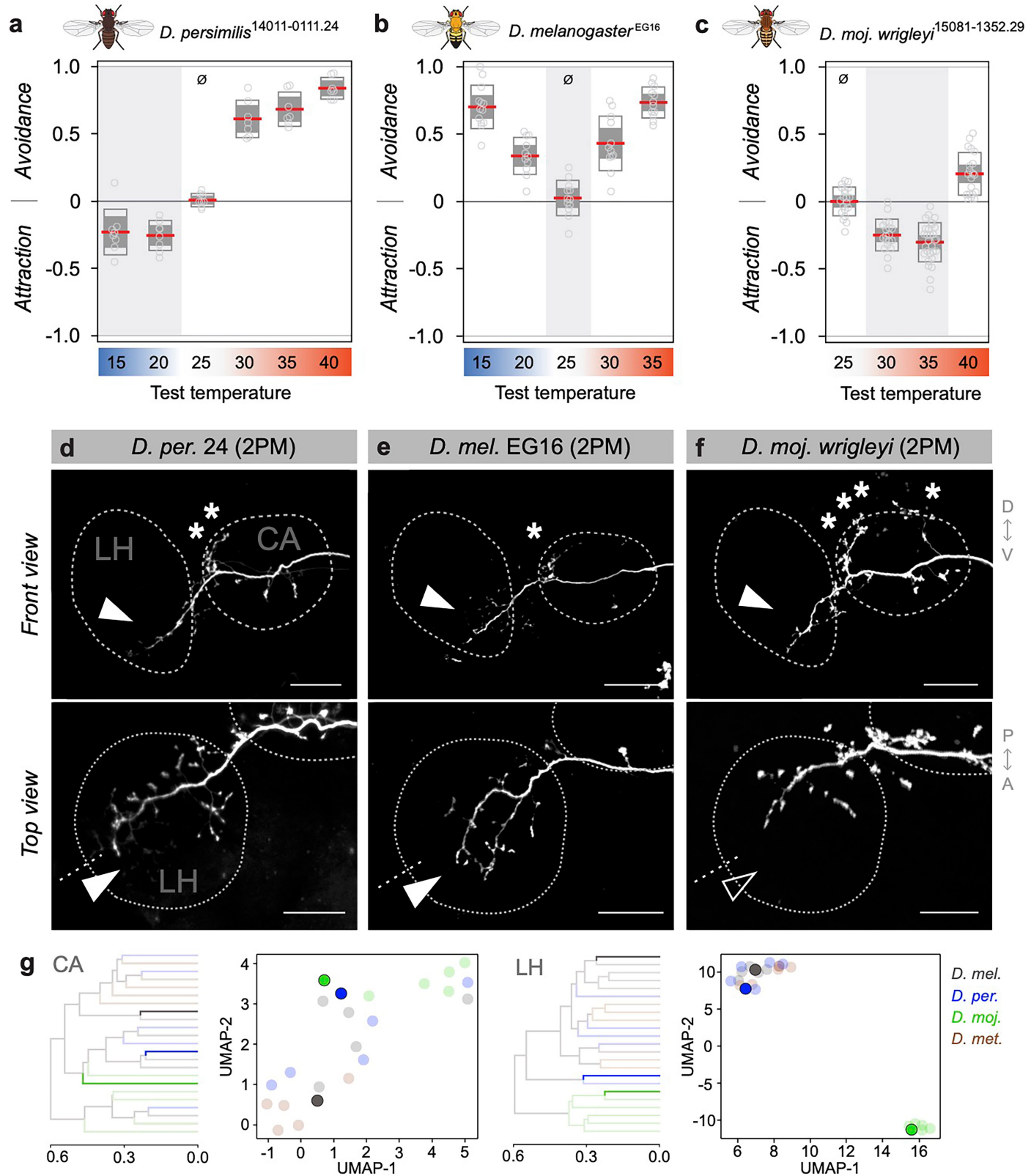
(d) A split-Gal4 driver exclusively expressed in TLHON-II (maximum projections of 2-photon z-stacks of the brain and VNC of TLHON-II-Gal4>GFP animal). Scale bars = 25 μm. (e) Genetic silencing using TLHON-II:Gal4>Kir2.1 impacts heat avoidance (*p < 0.05, 2-way ANOVA, p = [0.748, 1.95e-3, 4.15e-5, 4.91e-7] for test temperatures 25, 30, 35, and 40, respectively) (f) Optogenetic activation via TLHON-II:Gal4>CsChrimson is sufficient to induce avoidance of red light (*p < 0.05 indicates significant difference from zero in two-way one sample t-test, p = [0.440, 0.983, 2.54e-5] for Gal4/+, UAS/+, and Gal4>UAS, respectively). (in e-f red lines=mean, grey boxes=one standard deviation, empty boxes=95% confidence interval for the mean, circles=groups of 15 and 25 flies each for e and f, respectively; N = 8 and 9 groups/condition for e and f, respectively). Abbreviations: Lateral Horn, LH; Calyx, CA; Posterior Antennal Lobe, PAL; Mushroom Body, MB; Superior Medial Protocerebrum, SMP.



Extended Data Fig. 6 | Labelling olfactory projections in the *D. mojavensis* brain reveals largely conserved Lateral Horn organization. (a) Schematic of the *Drosophila* olfactory system. Olfactory Receptor Neurons (ORNs) send axons to the Antennal Lobe (AL) where they connect with specific second-order Olfactory Projection Neurons (OPNs) that relay information to higher brain centers such as the CA and LH. The ORN/OPN circuit of glomerulus DM1 is schematized next to an EM reconstruction of the *D. melanogaster* DM1 OPN. (b) Loading of dextran-conjugated dyes on the antennal nerve allows visualization of stochastic subsets of ORN axons that can be recognized due to the stereotype position of glomeruli (a *D. mojavensis* DM1 is shown) and used as a target for electroporation. (c) Innervation of the CA and LH by DM1-OPN is identical in *D. mojavensis* (in neuronal reconstructions and 2-photon z-stacks) as compared to *D. melanogaster* (EM reconstructions). Stacks from three

individual *D. mojavensis* flies are shown to highlight stereotypy of innervation (right). (d) To label both olfactory and thermosensory projections in the same brain, a red dye was first used to load the aristal nerve while a green dye was later used to load the antennal nerve (see methods for details). This allows independent visualization of PAL and AL glomeruli as targets for 2-color dye-labelling experiments. (e) 2-photon imaging demonstrates that DM1-PN innervation (white, labelled with AlexaFluor™ 594 dye) of the LH is essentially identical in *D. mojavensis* as compared to *D. melanogaster* (green, EM). In contrast, *D. mojavensis* TPN-V innervates only the posterior LH (red, labelled with AlexaFluor™ 488 dye), while the *D. melanogaster* TPN-V counterpart innervates more broadly (red, EM). Abbreviations: Lateral Horn, LH; Calyx, CA; Antennal Lobe, AL; Posterior Antennal Lobe, PAL; Olfactory Receptor Neurons, ORNs; Olfactory Projection Neurons, OPNs. Scale bars = 25 μm.

Article



Extended Data Fig. 7 | See next page for caption.

Extended Data Fig. 7 | Temperature preference behavior and TPN-V innervation are species-specific and consistent across populations.

(**a–c**) Preference indexes measured from additional strains of *D. persimilis*, *D. melanogaster*, and *D. mojavensis*, demonstrate consistent behavior within populations of the same species (compare to data shown in Fig. 1b–d, based on different strains -see methods). (**a**) A *D. persimilis* strain from Santa Rosa, California (strain 24) (N = 8,8,8,7,7 groups of 15 flies for test temperatures 15, 20, 25, 30, 35, and 40 °C, respectively). (**b**) A wild-derived *D. melanogaster* strain from Egypt (EG16; N = 13,11,12,12 groups of 15 flies for test temperatures 15, 20, 25, 30, and 35 °C, respectively). (**c**) A *D. mojavensis wrigleyi* strain from Catalina Island (*D. m. wrigleyi* is a subspecies of *D. mojavensis*; N = 20,19,18,20 groups of 15 flies for 25, 30, 35, and 40 °C, respectively) (**d–f**) 2-photon z-stacks of dye-labelled TPN-V in each of the three strains shows consistent anatomy

within species (compare to data shown in main Figs. 4 and 5, based on different strains of the same species -see methods). (**g**) A distance matrix of reconstructions (see methods) shows additional strains cluster by species (highlighted branches/datapoints represent additional strains generated from 2P images in **d–f**, whereas greyed out ones are re-plotted from Fig. 5). Abbreviations: Lateral Horn, LH; Calyx, CA. Scale bars = 25 μm. Asterisks: lateral Accessory Calyx (lACA). Arrowheads = ventral anterior LH, the dotted line is for reference. (In **a–c**: red lines=mean, filled boxes=one standard deviation, empty boxes=95% CI of the mean, empty circles=groups of flies, grey shading = approx. favorite thermal range, and Ø denotes preference indexes not significantly different from zero in two-tail one sample t-test; p < 0.05, p = [6.30e-3, 3.33e-4, 0.747, 2.47e-5, 7.67e-6, 1.55e-7] for **a**, p = [2.22e-9, 9.38e-6, 0.488, 1.34e-5, 1.76e-10] for **b**, and p = [0.888, 3.66e-8, 1.58e-7, 1.13e-5] for **c**).

Reporting Summary

Nature Portfolio wishes to improve the reproducibility of the work that we publish. This form provides structure for consistency and transparency in reporting. For further information on Nature Portfolio policies, see our [Editorial Policies](#) and the [Editorial Policy Checklist](#).

Statistics

For all statistical analyses, confirm that the following items are present in the figure legend, table legend, main text, or Methods section.

n/a Confirmed

- The exact sample size (n) for each experimental group/condition, given as a discrete number and unit of measurement
- A statement on whether measurements were taken from distinct samples or whether the same sample was measured repeatedly
- The statistical test(s) used AND whether they are one- or two-sided
Only common tests should be described solely by name; describe more complex techniques in the Methods section.
- A description of all covariates tested
- A description of any assumptions or corrections, such as tests of normality and adjustment for multiple comparisons
- A full description of the statistical parameters including central tendency (e.g. means) or other basic estimates (e.g. regression coefficient) AND variation (e.g. standard deviation) or associated estimates of uncertainty (e.g. confidence intervals)
- For null hypothesis testing, the test statistic (e.g. F , t , r) with confidence intervals, effect sizes, degrees of freedom and P value noted
Give P values as exact values whenever suitable.
- For Bayesian analysis, information on the choice of priors and Markov chain Monte Carlo settings
- For hierarchical and complex designs, identification of the appropriate level for tests and full reporting of outcomes
- Estimates of effect sizes (e.g. Cohen's d , Pearson's r), indicating how they were calculated

Our web collection on [statistics for biologists](#) contains articles on many of the points above.

Software and code

Policy information about [availability of computer code](#)

Data collection

Voltage clamp recordings were acquired with Axograph software v. 1.5.4 (Axon Instruments). For two-photon imaging experiments, images were acquired using Bruker PrairieView software (v. 5.2). For confocal imaging experiments, images were acquired using LSM 5 PASCAL Software (v. 4.0 SP2). 2-choice temperature preference behavior videos were acquired using MATLAB (v. R2023a), and 2-choice optogenetic preference behavior videos were acquired using a Raspberry Pi Camera with picamera Python package (v. 1.12) and Adafruit CircuitPython NeoPixel module (v. 6.3.8).

Data analysis

Two-photon images were processed and analyzed using Fiji (ImageJ2, v. 2.14.0), Fiji plugins (Segmentation Editor; Simple Neurite Tracer; CMTK Registration GUI), neuTube software (v. 1.0), Vaa3D (v. 1.1.2), Cajal Python package (v. 1.0.3), and scikit-learn Python package (v. 1.5.0). Confocal images were processed and analyzed using Fiji (ImageJ2, v. 2.14.0). D. melanogaster brain volume images, neuron skeletons, and brain region ROIs were downloaded from the Hemibrain:v1.2.1 dataset (from neuPrint database) and analyzed in Paraview (v. 5.11.0). For analysis of RNA sequencing data the following open source code was used: STAR (v. 2.7.9a), Samtools (v. 1.13), and R (base package, build 576). Data from voltage clamp recordings were analyzed offline using Axograph software v. 1.5.4 (Axon Instruments) and in Igor Pro (v. 6.37). All 2-choice behavior videos were processed and analyzed using MATLAB (v. R2023a) and the “notBoxPlot” function (v. 1.31.0). Multiple sequence alignment of Gr28b.d protein sequence was generated using Clustal Omega (v. 1.2.3) in the Geneious Prime software (v. 2023.1.1).

For manuscripts utilizing custom algorithms or software that are central to the research but not yet described in published literature, software must be made available to editors and reviewers. We strongly encourage code deposition in a community repository (e.g. GitHub). See the Nature Portfolio [guidelines for submitting code & software](#) for further information.

Data

Policy information about [availability of data](#)

All manuscripts must include a [data availability statement](#). This statement should provide the following information, where applicable:

- Accession codes, unique identifiers, or web links for publicly available datasets
- A description of any restrictions on data availability
- For clinical datasets or third party data, please ensure that the statement adheres to our [policy](#)

All data in this paper are available in the main text or as supplementary materials and source data are provided. Gr28b.d coding sequences from *D. persimilis* (GenBank OQ624956), *D. mojavensis* (GenBank OQ621410), and *D. mettleri* (GenBank PP885916) are deposited in Genbank. Raw read sequences from RNAseq with *D. mojavensis aristae* are uploaded to the NCBI Sequence Read Archive (SRA) with the BioProject ID: PRJNA948454. The following databases were also used: EM Hemibrain:v1.2.1 (<https://neurprint.janelia.org/>).

Research involving human participants, their data, or biological material

Policy information about studies with [human participants or human data](#). See also policy information about [sex, gender \(identity/presentation\), and sexual orientation](#) and [race, ethnicity and racism](#).

Reporting on sex and gender

n/a

Reporting on race, ethnicity, or other socially relevant groupings

n/a

Population characteristics

n/a

Recruitment

n/a

Ethics oversight

n/a

Note that full information on the approval of the study protocol must also be provided in the manuscript.

Field-specific reporting

Please select the one below that is the best fit for your research. If you are not sure, read the appropriate sections before making your selection.

Life sciences

Behavioural & social sciences

Ecological, evolutionary & environmental sciences

For a reference copy of the document with all sections, see nature.com/documents/nr-reporting-summary-flat.pdf

Life sciences study design

All studies must disclose on these points even when the disclosure is negative.

Sample size

To choose sample sizes, preliminary data were used to assess the variance for each experiment. While sample sizes were not predetermined, they were kept consistent across experiment type. Additionally, sample sizes are comparable to recent studies for behavior data (e.g. Frank et al, 2015; Jouandet et al, 2023; Kim et al, 2021) electrophysiology measurements (e.g. Arenas et al, 2017; Nguyen et al, 2022; Hiro et al, 2023), and neuron dye fills in non-*D. melanogaster* species (e.g. Ellis et al, 2024).

Data exclusions

No data were excluded from the analysis.

Replication

For the electrophysiological experiments, repeated measurements were taken from a number of cells and cell lines as indicated in the corresponding Figure legend of panels. For behavior, experiments were replicated in independent biological replicates across days and months, with groups of 15-20 flies with sample sizes indicated in the corresponding Figure legend for each panel. In cases where representative images are depicted, experiments were repeated with a minimum of 5 animals, and for independently performed dye fills the summary statistics of the number of biological replicates are indicated in Extended Data Figure 4 for each condition. All data were successfully replicated.

Randomization

For behavior data, individual animals from each genotype/treatment were randomly selected from groups. Groups being compared were randomly interleaved when running behavior experiments each day, and behavior data were performed and analyzed by different experimenters. For electrophysiology experiments, cells were screened for GFP marker expression and then randomly chosen for recording from a dish of cells. For imaging and dye fill experiments, individual biological replicates were randomly chosen from groups for each condition.

Blinding

The experimenters were not blind to genotypes. Blinding was not relevant for behavior and electrophysiology experiments as data analysis was automated eliminating potential operator bias. For dye filling experiments, blinding was not possible as the experimenter was guided by GFP fluorescence or a combination of fluorescent dyes (GFP, tdTomato, AlexaFluor 488, TexasRed), respectively. Reconstructions and data analysis were automated eliminating potential operator bias.

Reporting for specific materials, systems and methods

We require information from authors about some types of materials, experimental systems and methods used in many studies. Here, indicate whether each material, system or method listed is relevant to your study. If you are not sure if a list item applies to your research, read the appropriate section before selecting a response.

Materials & experimental systems		Methods	
n/a	Involved in the study	n/a	Involved in the study
<input type="checkbox"/>	<input checked="" type="checkbox"/> Antibodies	<input type="checkbox"/>	<input type="checkbox"/> ChIP-seq
<input type="checkbox"/>	<input checked="" type="checkbox"/> Eukaryotic cell lines	<input type="checkbox"/>	<input type="checkbox"/> Flow cytometry
<input checked="" type="checkbox"/>	<input type="checkbox"/> Palaeontology and archaeology	<input type="checkbox"/>	<input type="checkbox"/> MRI-based neuroimaging
<input type="checkbox"/>	<input checked="" type="checkbox"/> Animals and other organisms		
<input checked="" type="checkbox"/>	<input type="checkbox"/> Clinical data		
<input checked="" type="checkbox"/>	<input type="checkbox"/> Dual use research of concern		
<input checked="" type="checkbox"/>	<input type="checkbox"/> Plants		

Antibodies

Antibodies used

Mouse anti-nc82 (AB_2314866, DSHB), Chicken anti-GFP (ab13970, abcam), AlexaFluor® 488 donkey anti-chicken IgY (AB_2340375, Jackson ImmunoResearch Laboratories, Inc), and AlexaFluor® 594 donkey anti-mouse IgY (AB_2340854, Jackson ImmunoResearch Laboratories, Inc).

Validation

All primary antibodies were validated by the manufacturer. The mouse anti-nc82 (DSHB) antibody was validated with IHC, IHC-IF, ICC, and IF. Cited in 1019 publications, and further details are described on the manufacturer's website. The chicken anti-GFP (ab13970, abcam) antibody was validated with WB, ICC, and IF. Cited in over 3820 publications, further details are described on the manufacturer's website.

Eukaryotic cell lines

Policy information about [cell lines and Sex and Gender in Research](#)

Cell line source(s)

HEK293T cells were sourced from ATCC (CRL-3216). S2R+ cells were sourced from the Drosophila Genomics Resource Center (DGRC Stock 150, RRID:CVCL_Z831).

Authentication

For the HEK293T cell line, ATCC performed authentication and quality-control tests before distribution with PCR amplification and Sanger Sequencing. Cited in 38367 publications, further details are described on the manufacturer's website. For the S2R+ cell line, DGRC performed authentication and quality-control tests before distribution with genome sequencing and transcriptome analysis via RNAseq. Cited in 718 publications, further details are described on the manufacturer's website. All cell lines used were at early passage number as shipped from the distributor. No further authentication tests were performed.

Mycoplasma contamination

The cell lines used were not tested for Mycoplasma contamination.

Commonly misidentified lines (See [ICLAC](#) register)

No commonly misidentified lines were used in this study.

Animals and other research organisms

Policy information about [studies involving animals; ARRIVE guidelines](#) recommended for reporting animal research, and [Sex and Gender in Research](#)

Laboratory animals

D. melanogaster (FL50), D. melanogaster (EG16), D. persimilis (14011-0111.51), D. persimilis (14011-0111.24), D. moj. mojavensis (15081-1352.47), D. moj. wrigleyi (15081-1352.29), and D. mettleri (15081-1502.13). All animals used in experiments were tested on 3-5 day post-eclosion male flies.

Wild animals

No wild animals were used in the study.

Reporting on sex

n/a

Field-collected samples

No field collected samples were used in the study.

Ethics oversight

No ethical approval was required because Drosophila melanogaster, D. mojavensis, D. persimilis, and D. mettleri were used as experimental animals.

Note that full information on the approval of the study protocol must also be provided in the manuscript.

Plants

Seed stocks

n/a

Novel plant genotypes

n/a

Authentication

n/a